Technical Document 2749
March 1995

Array Element Localization Using Broadband Pulses

T.J. Pastore

Technical Document 2749
March 1995

Array Element Localization Using Broadband Pulses

T.J. Pastore

NAVAL COMMAND, CONTROL AND
OCEAN SURVEILLANCE CENTER
RDT&E DIVISION
San Diego, California 92152-5001

K. E. EVANS, CAPT, USN
Commanding Officer

R. T. SHEARER
Executive Director

ADMINISTRATIVE INFORMATION

The work detailed in this document was performed by the Naval Command, Control and Ocean Surveillance Center, RDT&E Division, Applied Systems Branch, Code 532, for the Chief of Naval Operations. Funding was provided under program element .0603709N, accession number DN 302109, and subproject S0214.

Released by
C. D. Metz, Head
Applied Systems Branch

Under authority of
D. W. Murphy, Head
Advanced Systems Division

PS

EXECUTIVE SUMMARY

This report describes our procedure and initial study of the feasibility and practicality of using a frequency modulated (FM) chirp to perform a fine positional localization of hydrophone elements of a passive array. Results are analyzed with respect to variation based on direction of the sound source relative to the array and the ratio of sample rate to array frequency. Results show that the measurements are not consistent enough that a single measurement can be taken and used with great confidence. However, averages of about half a dozen measurements appear to have sufficient consistency.

Extraneous sources of acoustic energy, which were not planned or controlled in the test setup, are shown to be of comparable utility in localization of the array elements.

CONTENTS

Figures

Tables

INTRODUCTION

The objective of this document is to address the feasibility and practicality of using an FM chirp to determine, on a fine scale, the location of individual elements of a linear underwater acoustic array.

The principle was proven to be effective in controlled conditions based on a test conducted in January 1994 . In this earlier test, an eight–element array was used with similar signals in approximately 40 feet of water in San Diego Bay. This document relates to the first attempt to use this method in water that is deeper than diver depth (so the straightness of the array cannot be directly assured or verified). Since signals spanning a longer time were used in this test, the results are not directly comparable with the earlier test. However, the signals used in both tests had the same bandwidth and should achieve the same resolution.

TEST SETUP RELEVANT HARDWARE

The two arrays used in this test consisted of a compound array (nesting a 640–Hz array within a 160–Hz array) and a simple 160–Hz array separated by 1 km center to center. The total number of elements in the two arrays was originally to have been 64.

Digitization and telemetry of the data from each hydrophone was accomplished in eight nodes, each handling data from eight hydrophones. Acoustic data were digitized to 14–bits at a sample rate of 3276.8 Hz. The first hydrophone from each node was sampled simultaneously, the second hydrophone from each node was sampled 12 μsec later, and each node's third hydrophone was sampled 12 μsec after that, etc. See figure 1 for a sampling timing diagram. In this way, the timing skew between channels (hydrophones) is known, and has a maximum value of 7 X 12 μsec = 84 μsec. In terms of the sample period, $\tau = 1/3276.8 = 305$ μsec, so the maximum skew is about 27.5% of a sample period.

Prior to the deployment, six of the hydrophones were eliminated due to manufacturing problems, and the spacing was adjusted accordingly. Upon deployment, certain other hydrophones stopped working or existed with reduced functionality. For this reason, there are a few ways in which the hydrophones can reasonably be numbered. Refer to figure 2 for an explicit diagram of the arrays and interelement spacing. The primary means of labeling that shall be used is sequential numbering of the 58 physically present hydrophones, starting at the shore end.

The arrays were laid along the bottom as straight as possible along a line of bearing of 135° true, to the southwest of Point Loma, San Diego, CA. The water depth in this area is approximately 90 meters. See figure 3.

Two active sound sources were also deployed on the ocean floor. Initially, one was placed normal to the high–frequency array, and one was placed in–line between the arrays. The one normal was later placed at a location normal to the low–frequency array. The fine layout of the arrays and sources is shown in figure 4. These sources emitted the FM signals at scheduled times. Two different chirps were used. The high–bandwidth chirp was 0.25–second long, and frequency dropped linearly from 1280 Hz to 280 Hz. The low–bandwidth chirp was also 0.25–second long, and frequency dropped linearly from 640 Hz to 140 Hz. The high–bandwidth chirp was transmitted at the top of the minute, and the low–bandwidth at 40 seconds after. Timing accuracy was achieved by a calibration with a Global Positioning System (GPS) receiver before the source was deployed.

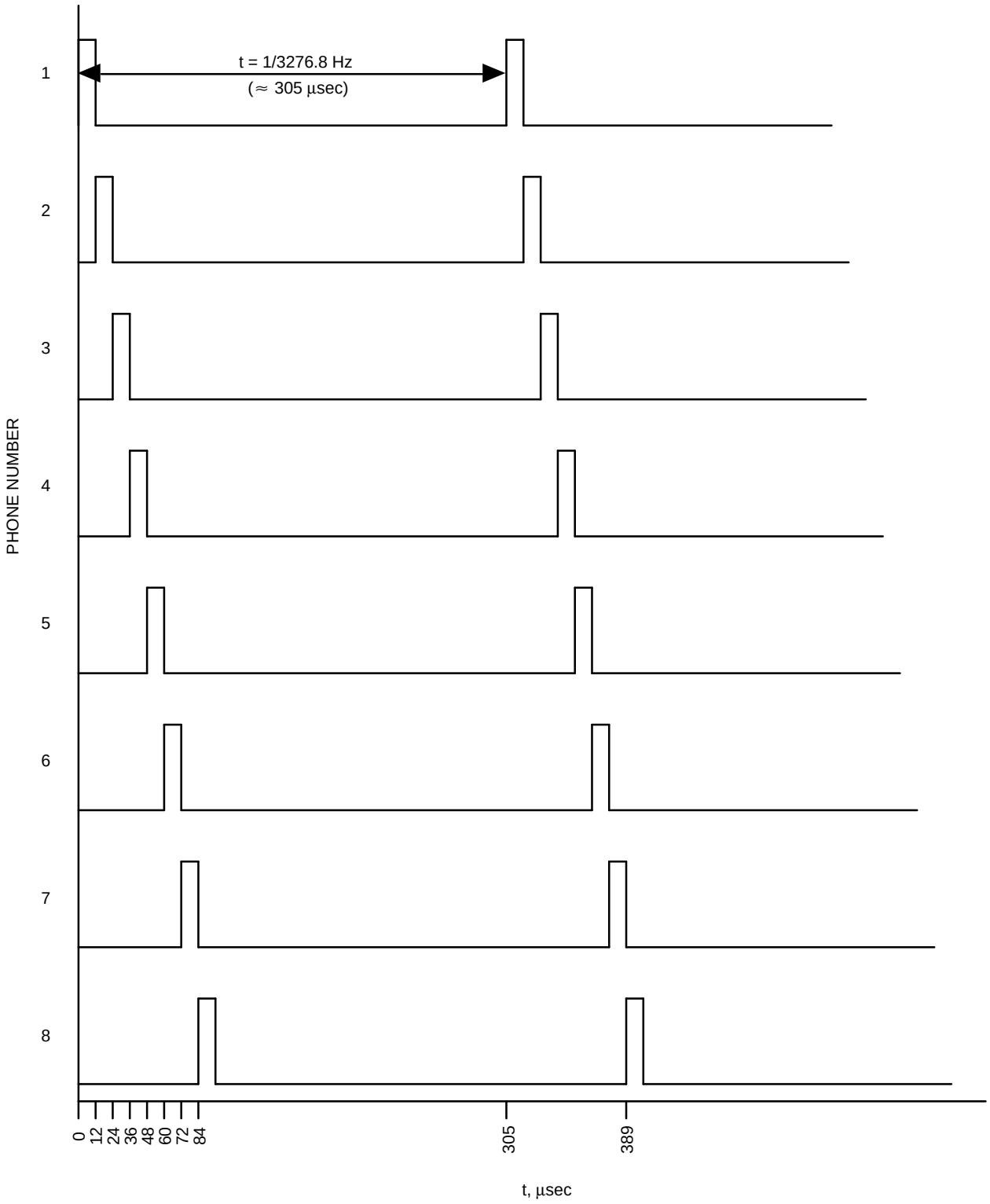

Timing for each of eight telemetry nodes. Phone 1 from each node is simultaneous.

Figure 1. Timing diagram.

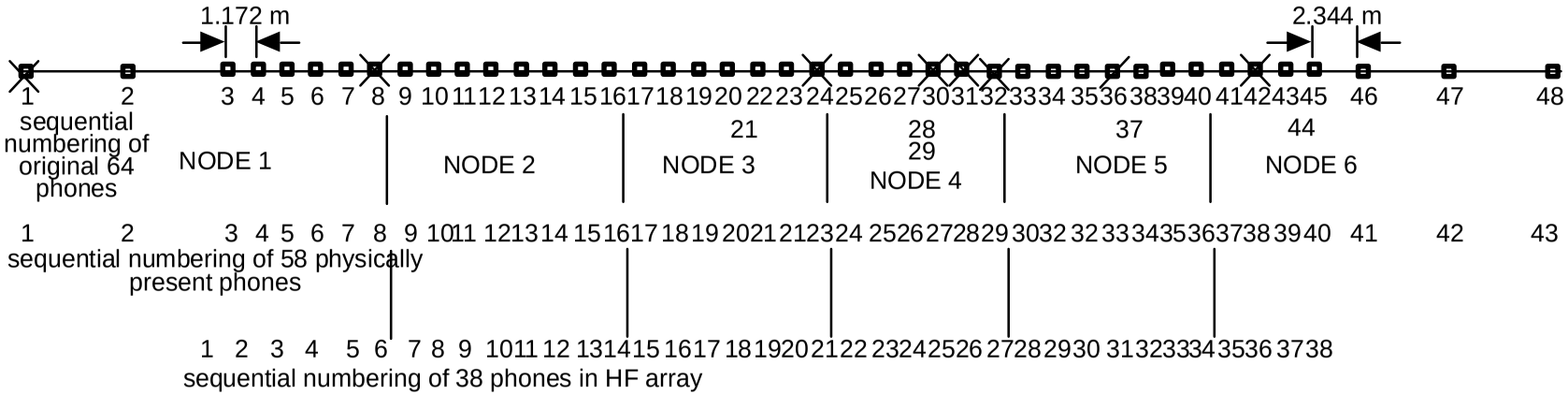

= BAD PHONE (7 PLACES)

= MARGINAL PHONE (1 PLACE)

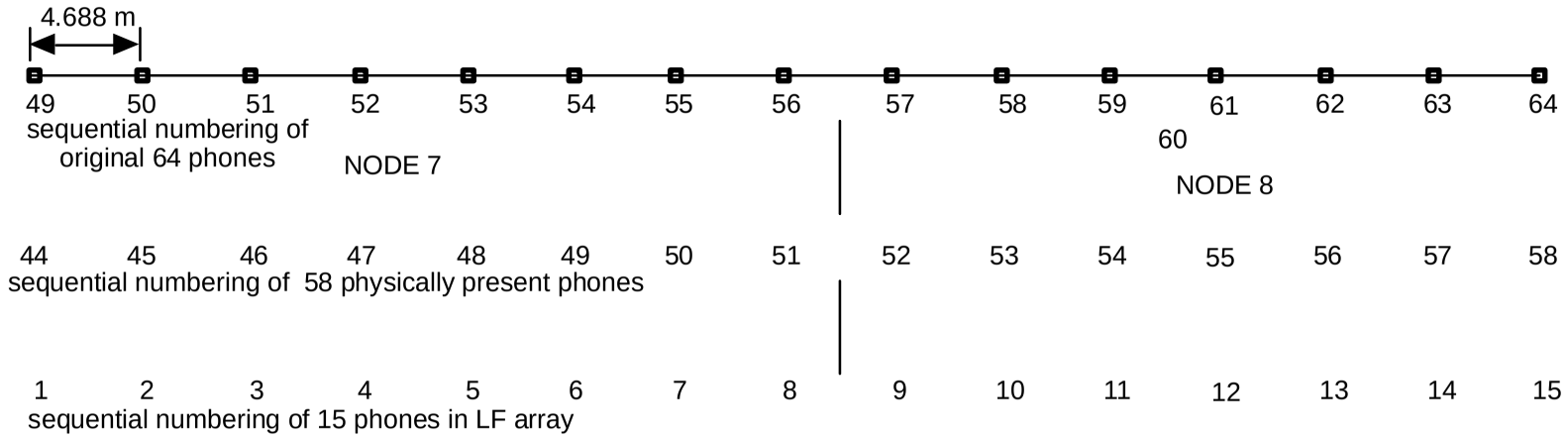

Figure 2. String layout.

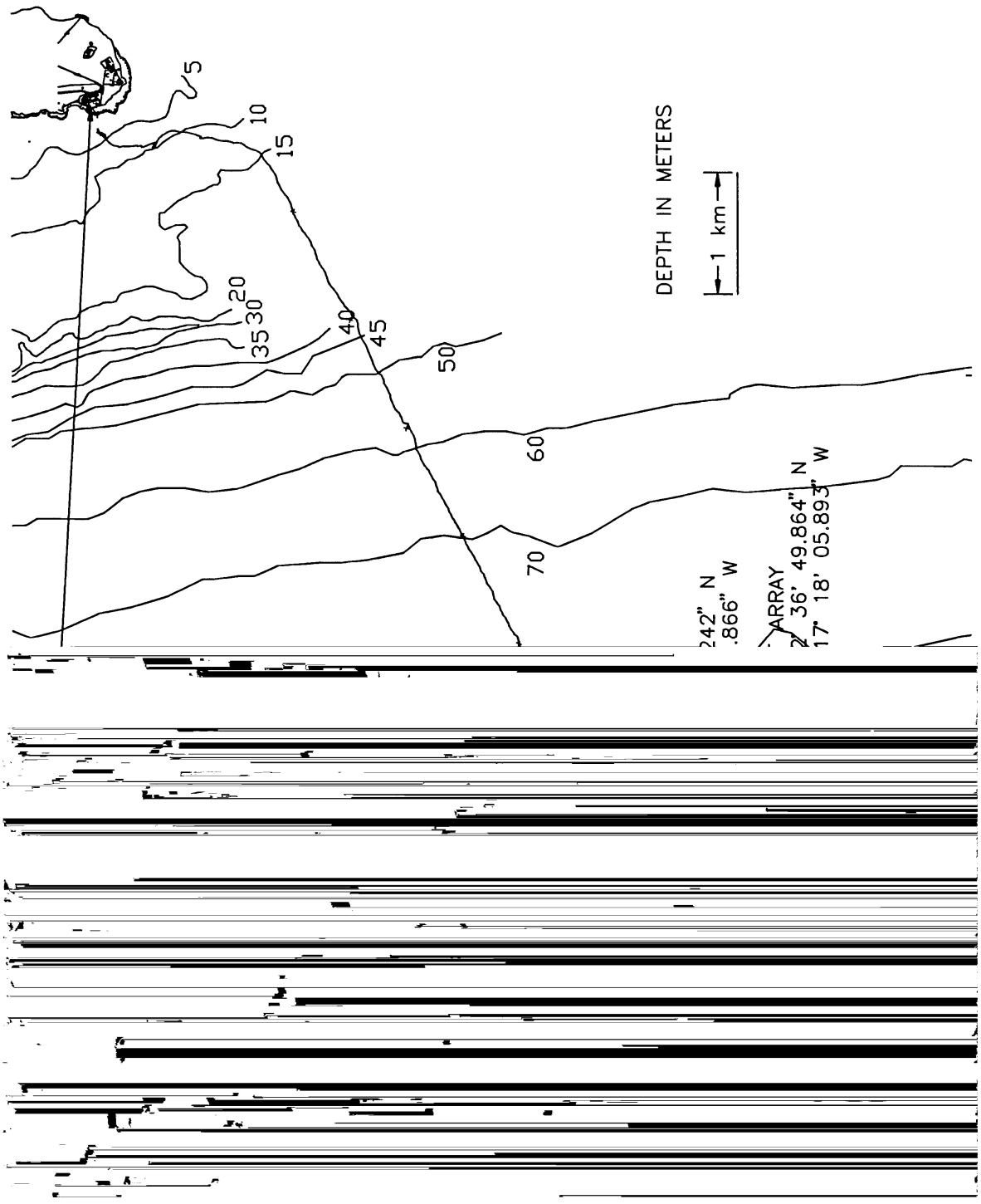

Figure 3. EDM1-E deployment 14 SEP 1994.

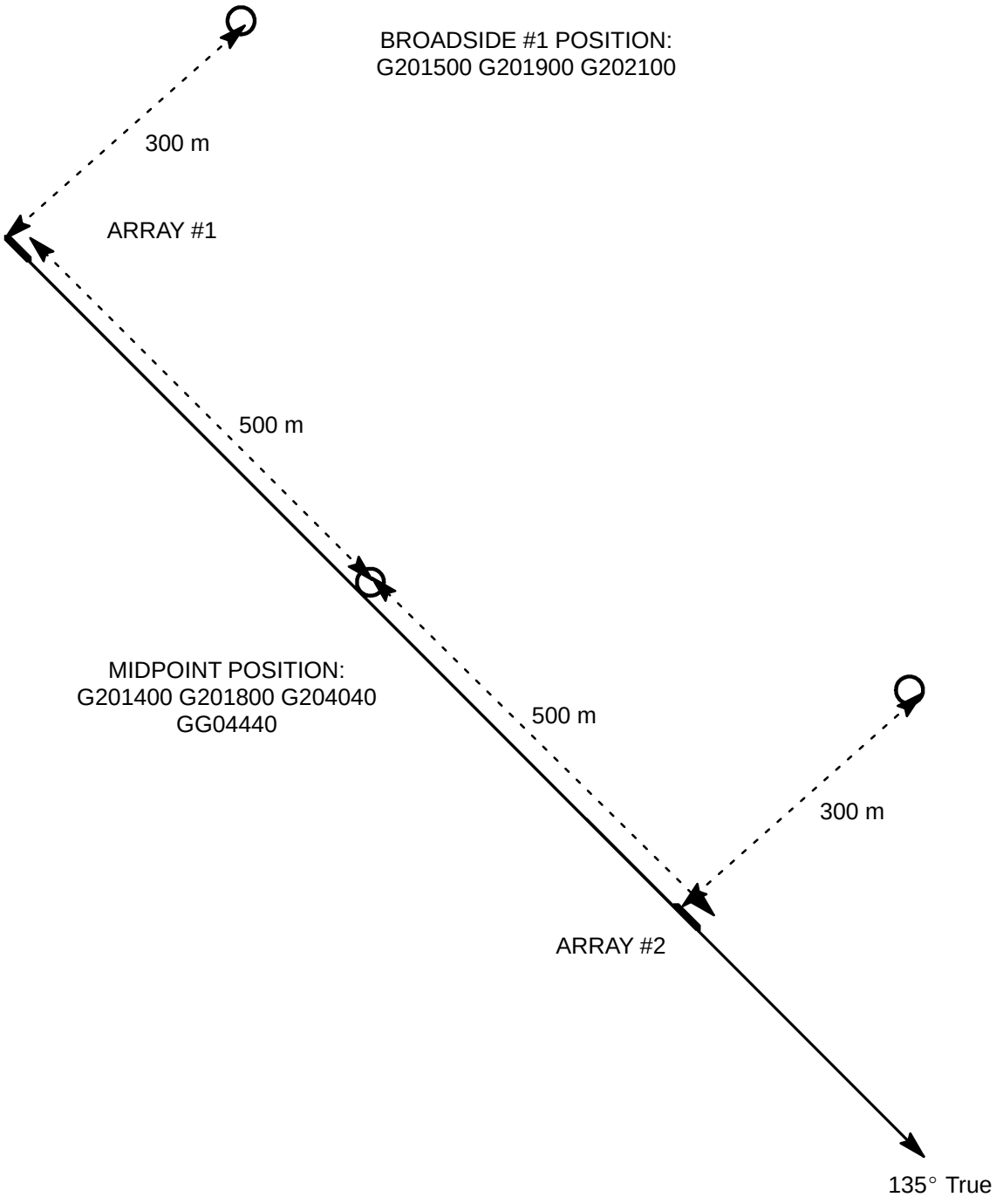

Figure 4. Approximate source locations.

The recording system was implemented in a 486 computer. It was capable of recording up to 2.5 seconds of data, beginning at a particular time specified as HH:MM:SS coordinated universal time. The recording computer had a full–time link to a GPS receiver. All data used for this report were recorded within a 2–hour period on the afternoon of 14 September 1994.

PROCEDURE

The relative delays between hydrophones were estimated using a seven–step process that is detailed in this section. An eighth step is also shown, which converts delays to angle of arrival.

1. Pare down the matrix.

The data was initially stored as a matrix **A** of N X 64, where N is the number of samples, usually between 6000 and 8000. Since the sound sources were always within about 1000 meters of the arrays, only a few thousand samples were necessary to acquire the signals, and the later samples were eliminated. Also, the data matrix was 64 columns wide, corresponding to the original 64 hydrophones on the string. The 21st, 28th, 29th, 37th, 44th, and 60th columns were eliminated, since these correspond to hydrophones that were no longer physically present when the array was deployed. This leaves the raw data in a N X 58 matrix, with N varying on a file by file basis from 1536 to 4096. This matrix was **B** such that,

$$\mathbf{B} = \mathbf{A}_{\forall\ j \neq \{21,28,29,37,44,60\}}$$

2. Zero out the bad channels.

As seen in figure NO TAG, there are seven hydrophones that were not producing any useful signal. So they would not influence the statistics, these channels were replaced with zeros. At the same time phone #40 (of 58) was inverted, which compensates for its being wired 180° out of phase.

The channels were zeroed instead of being removed because they are useful to retain as place–holders. An array with uniform spacing can still be formed with the inclusion of these virtual phones.

These operations can be easily accomplished by an element–by–element multiplication of row of **B** by a "correction vector" **c**.

$$\mathbf{c} = [0\ 1\ 1\ 1\ 1\ 1\ 1\ 0\ 1\ 1 \ldots 1\ 0\ 1\ 1\ 1\ 1\ 0\ 0\ 0\ 1\ 1\ 1\ 1\ 1\ 1\ 1\ 1\ 0\ 1\ {-1}\ 1 \ldots 1]$$

$$\mathbf{B}_i = \mathbf{B}_i \bullet \mathbf{c}\ ,\ \forall i$$

3. Replica correlation.

The intended method of postprocessing was to filter the received signal using a matched filter based on a replica of the transmitted signal, and measure the time delays between peaks of the output to determine relative positions of the hydrophones. By doing this with signals from two (or more) sources at different aspect angles, a two-dimensional rendering of the array element positions can be obtained.

The first practical problem was obtaining a suitable replica. There are three possible options:

a. Mathematically generated signal,

b. Recorded replica,

c. Using one of the received channels as a replica.

A mathematically generated signal is not a very good representation of the signal as received by the array, since by the time it is received it has been distorted by the projection transducer, the transmission through a few hundred meters of seawater, and (minimally) by the receiving hydrophone.

A recording of the test signals was taken in a calibration pool. This high–fidelity recording yields a replica that is transformed by the transfer function of the projector. However, it was recorded at a distance of only 0.5 meter.

The drawback of using one of the received channels as a replica is the replica will then be tainted by any noise present at that channel at the time of the recording. Since the signal–to–noise ratio (SNR) is about 0 dB in some cases, this is a significant concern. Additionally, appropriate windowing of the signal is difficult in a case of little or no signal excess.

We investigated using each of the three methods. The criteria for choosing the preferred method is its ability to produce a sharp and distinct peak in the cross–correlation with secondary peaks minimized relative to the main peak. When appropriately windowed in time, the use of one of the channels as a replica produced the best results. The recorded signal and the mathematically pure signal were both inferior.

A two-step correlation was implemented to automate the process of choosing a window in time that contains the signal and to choose the "best" of the received channels as a replica. First, the time–reversed ideal chirp (**r**) was convolved with each column of **B**. The column of **B** that produced the "best match" (highest peak) was chosen as the replica and then convolved with the entire matrix. This "best" column of B was windowed in time to 0.3125 second (1024 samples) centered at the location of the highest peak. The result of this cross–correlation operation is called **D.**

$$C_{i0j0} = \max(\mathbf{r} * \mathbf{B})$$

$$\mathbf{b} = \mathbf{B}_{i:i=i0-\text{size}(\mathbf{r}) \text{ to } i0-\text{size}(\mathbf{r})+1024,j0}$$

$$\mathbf{D} = \mathbf{B} * \mathbf{b}$$

4. Find position of peaks.

The relevant information in the matrix **D** (output of the replica correlation) is simply the location of the peak of each column. This corresponds to the delay from the transmission of the pulse to the arrival at each hydrophone. The units are samples, with each sample representing 305 μsec.

$$\mathbf{d} = i{:}\mathbf{D}_{ij}=\max(\mathbf{D}_j),\ \forall j$$

5. Interpolate over dead hydrophones.

Each of the hydrophones that were zeroed out in step 2 gets a delay value equal to the arithmetic mean of the two adjacent hydrophones.

$$d_j=(d_{j+1} + d_{j-1})/2,\ j=8,23,27,28,29,38.$$

6. Normalize delays relative to first hydrophone in array.

The high–frequency array consists of hydrophones 3 through 40. The uniform low–frequency array consists of hydrophones 44 through 58. These will be considered separately, so these two subsets of **d** are separated out, and then normalized so the first element is 0. Thus, the entire vector takes on the meaning "delay relative to first hydrophone."

$\mathbf{h} = d_{j:j=3 \text{ to } 40}$
$\mathbf{l} = d_{j:j=44 \text{ to } 58}$
$h_j = h_j - h_1, \ \forall j$
$l_j = l_j - l_1, \ \forall j$

At this point, consider the anticipated response of the row vectors **h** and **l** (high– and low–frequency arrays). First, suppose the arrays are perfectly straight. (In fact, if this were the case, this exercise would be unnecessary, but it does provide an adequate first–order approximation.) If the distance between the sound source and the array is large, then the wavefront impinging on the array can be approximated as a plane wave. This way, the delay between any two equally spaced hydrophones is the same. In the case where the source is located along the line of the array, the delays between arrivals will be maximized, and if the source is broadside to the array, the delays would be identically zero.

More specifically, if the source is located at endfire (along the line of) the array, the predicted delays can be derived as follows. The spacing of the hydrophones is equal to half a wavelength ($\lambda/2$).

$$\lambda/2 = c/2f_a = cT_a/2,$$

where c is the speed of propagation in the medium, generally assumed to be 1500 m/sec, f_a is the frequency of the array, and T_a is the reciprocal $1/f_a$. The period of the array T_a in number of samples is simply the ratio of the sample rate f_s to the array frequency f_a.

$$T_a=f_s/f_a.$$

Thus, the time delay (in number of samples) between elements is

$$\lambda/2c = f_s/2f_a \quad = 2.56 \text{ for } f_a = 640 \text{ Hz},$$
$$= 10.24 \text{ for } f_a = 160 \text{ Hz}.$$

7. Find first order polynomial fit of the delay data.

Find the straight–line fit that best approximates the delay data in a least squares sense. If j is the hydrophone (column) number, then we want to find

$\mathbf{p_h} = [p_{h1} \ p_{h2}] : \sum_j(\mathbf{p_h} \bullet [j \ 1]' - h_j)^2$ is minimized.

for the high–frequency array, and similarly for the low–frequency array,

$\mathbf{p_l} = [p_{l1} \ p_{l2}] : \sum_j(\mathbf{p_l} \bullet [j \ 1]' - l_j)^2$ is minimized.

Note that in the ideal case of a source at endfire to a perfectly straight array in the direction of hydrophone number 1, the polynomials will be $\mathbf{P_h}$ = [2.56 –2.56], and $\mathbf{P_l}$ = [10.24 –10.24].

8. Convert slope of polynomial to angle of source.

The slope of the best–fit polynomial can be used to determine the angle from which the wavefront originated. The slope (p_1) is physically constrained to be less than $|f_s/2f_a|$. The angle can be found as:

$$\Theta = \pm((f_s/2f_a - p_1)/(f_s/f_a))\pi$$
$$= \pm((2.56 - p_{h1})/5.12)\pi, \text{ for the high–frequency array}$$
$$= \pm((10.24 - p_{l1})/20.48)\pi, \text{ for the low–frequency array}$$

Although the actual value of the angle is of interest, the first term of the polynomial, p_1, is important for purposes of visualization. If each element of the delay vector is divided by p_1, and the result is plotted against hydrophone number on the abscissa, then the slope is normalized, and recordings taken from different angles relative to the array can be overlaid and directly compared.

COMPARISON OF RESULTS

Table 1 shows a summary of each recording in the data set that was initially considered. No ground truth knowledge exists regarding the actual exact positions of the arrays. However, it is known that motion was negligible, based on the lack of acoustic interference that would have accompanied any motion of the acoustic elements. Thus, the best comparison that can be made is one of consistency of the measurements from one trial to the next. The reader is also invited to compare results from an alternate method of element location in Williams (1994).

Table 1. Summary of data files used in analysis.

Date	Name/Time	CHIRP	Location
9/14/94	G201400	HF	BETWEEN
9/14/94	G201500	HF	OFF HF ARRAY
9/14/94	G201800	HF	BETWEEN
9/14/94	G201900	HF	OFF HF ARRAY
9/14/94	G202100	HF	OFF HF ARRAY
9/14/94	G203100	HF	OFF HF ARRAY
9/14/94	G204040	LF	BETWEEN
9/14/94	G204440	LF	BETWEEN
9/14/94	G204540	LF	OFF HF ARRAY
9/14/94	G204840	LF	BETWEEN
9/14/94	G220100	HF	OFF LF ARRAY
9/14/94	G220140	LF	OFF LF ARRAY
9/14/94	G220500	HF	OFF LF ARRAY
9/14/94	G220540	LF	OFF LF ARRAY
9/14/94	G220900	HF	OFF LF ARRAY

Table 2 shows the results of the procedure described in the previous section applied to the applicable data. Not all of the chirps produced meaningful measurements on both arrays. Possibly some of these were missed due to a timing problem.

Table 2. Best fit polynomial delays and computed angle of sound sources.

Name/Time	Location	Array	P1	ABS(Angle)
G201400	BETWEEN	HF	–2.4668	177
G201400	BETWEEN	LF	9.3643	8
G201500	OFF HF ARRAY	HF	–0.344	102
G201500	OFF HF ARRAY	LF	9.1857	9
G201800	BETWEEN	HF	–2.1695	166
G201800	BETWEEN	LF	9.5	7
G201900	OFF HF ARRAY	HF	–0.3485	102
G201900	OFF HF ARRAY	LF	9.3643	8
G202100	OFF HF ARRAY	LF	9.7929	4
G204040	BETWEEN	HF	0.1347	85
G204440	BETWEEN	LF	–2.8857	115
G220100	OFF LF ARRAY	HF	–1.9013	157
G220500	OFF LF ARRAY	LF	–9.1429	170
G220540	OFF LF ARRAY	LF	–9.0321	169
G220900	OFF LF ARRAY	LF	–2.975	116

Figures 5 through 10 show relative delay versus phone number for the high-frequency array, and figures 11 through 19 show relative delay versus phone number for the low-frequency array. The title on these plots refer to the time the data trial was recorded. Refer back to figure 4 for a layout of the arrays with the approximate source locations.

If the slope is normalized as was described in step 8 of the procedure section, all trials on a given array can be viewed on a common set of axes for comparison. Figure 20 shows the six data trials on the high–frequency array, and figure 21 shows the nine data trials on the low–frequency array.

DIRECTION OF SOURCE

The overwhelming conclusion based on direction of the source is that a direction closer to endfire (either end) gives better results. A measurement can only be made to one sample period, and this quantization is most detrimental when the arrival times are all close together. G204040 is the closest to broadside, whereas G201400 is closest to endfire on the high–frequency array. Figures 5 and 9 make this point clear.

The last column in table 2 shows the calculated angle of arrival of the chirp. Recall that since these are based on a perfect linear array, they are subject to a sign ambiguity. They are consistent with the actual deployed position of the sound source (which is not known to any great precision) in all cases except one — G204040.

Another interesting observation with regard to G204040 is shown in figure 22. This shows a subset of the lines in figure 20 (G201500, G201900, and G204040). As seen in table 2, all are nearly broadside, but the fact that G204040 appears as a mirror image of the other two indicates that it most likely originated from a southwesterly direction, while the others came from the northeast. The profound implication of this fact is that the process works well even when applied to signals other than the intended ones! This will be further addressed in a later section.

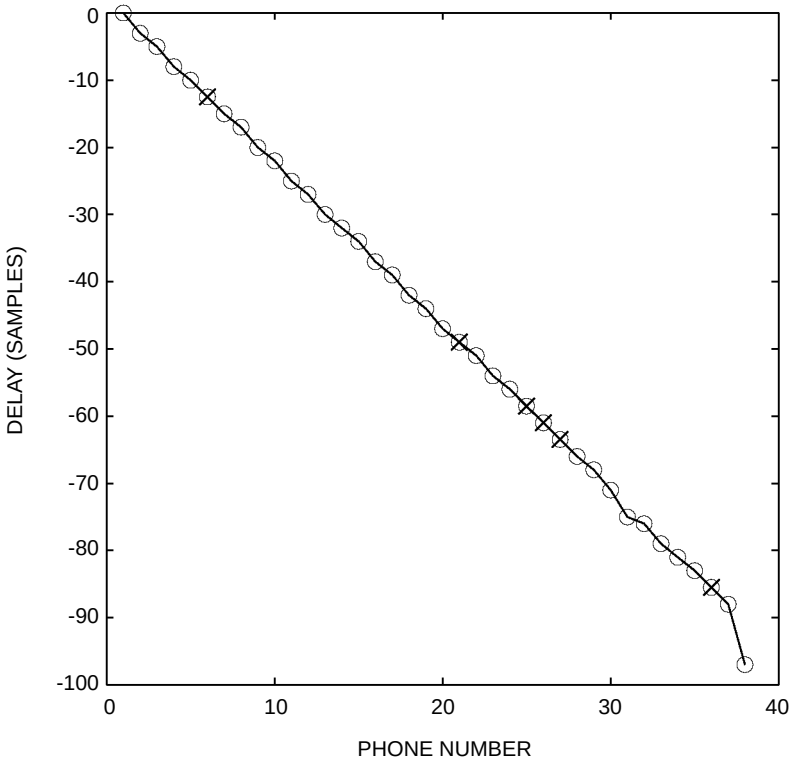

Figure 5. G201400, HF array.

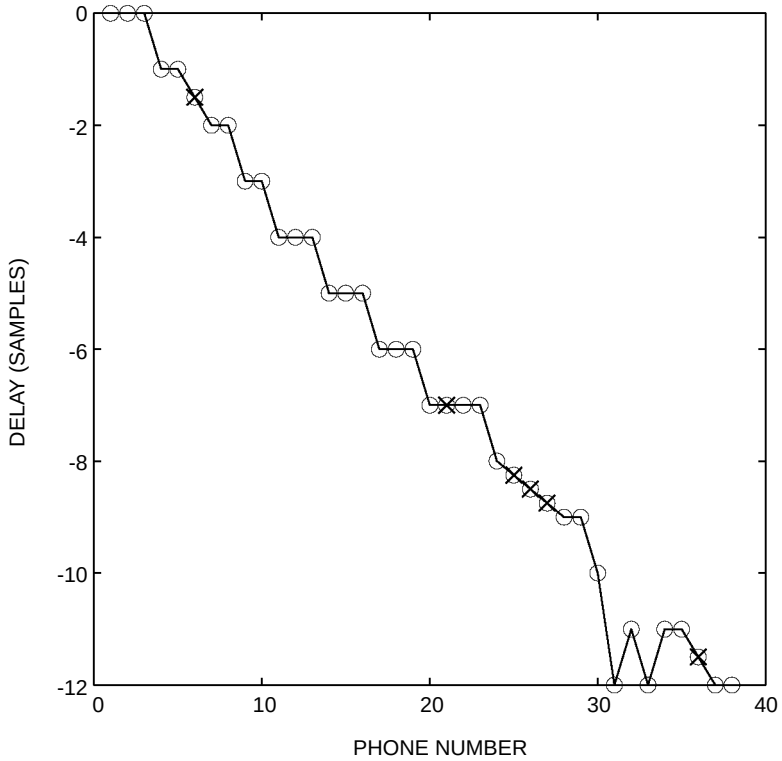

Figure 6. G201500, HF array.

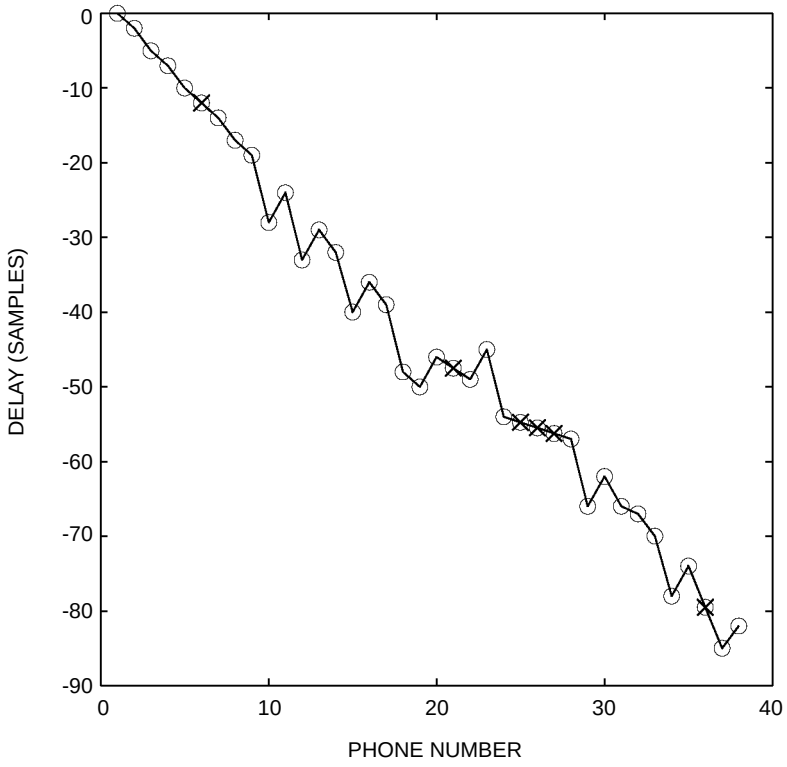

Figure 7. G201800, HF array.

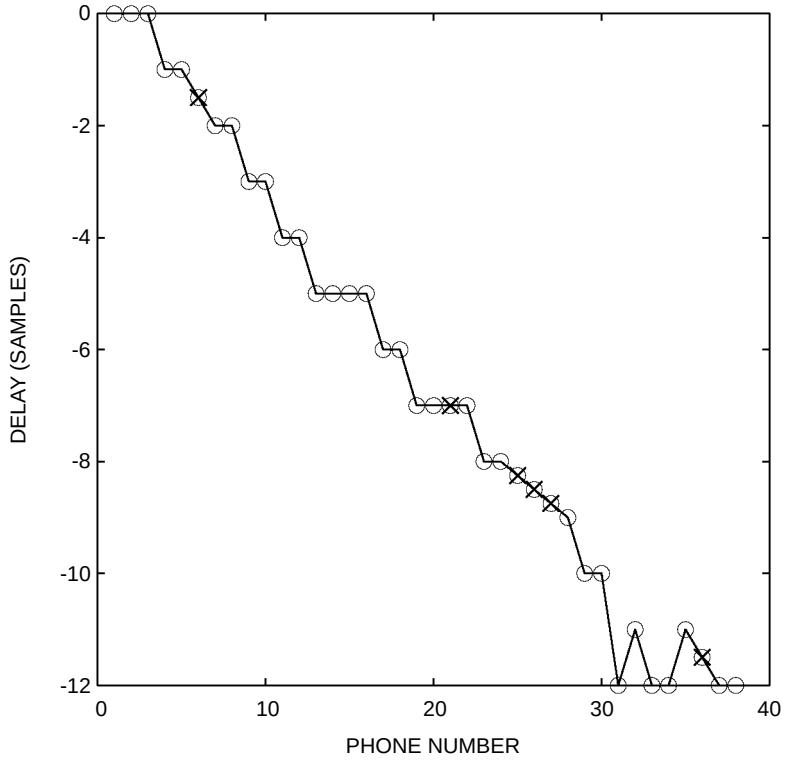

Figure 8. G201900, HF array.

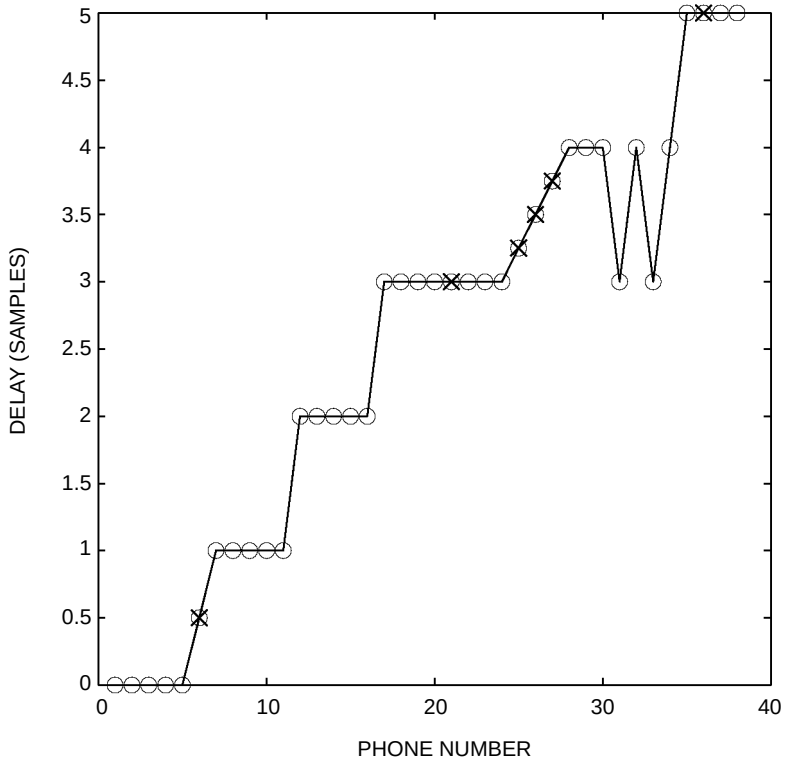

Figure 9. G204040, HF array.

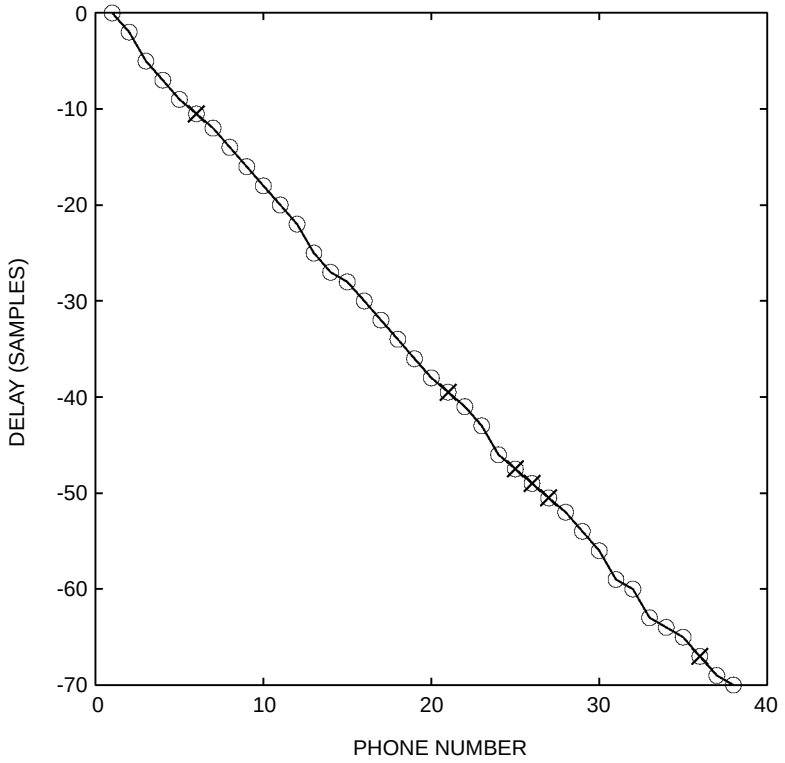

Figure 10. G220100, HF array.

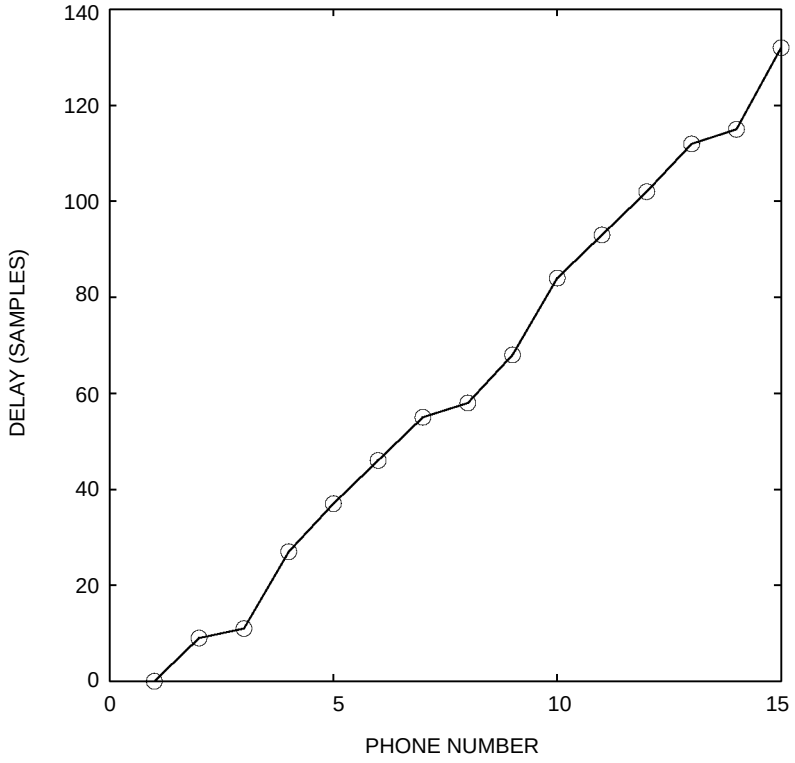

Figure 11. G201400, LF array.

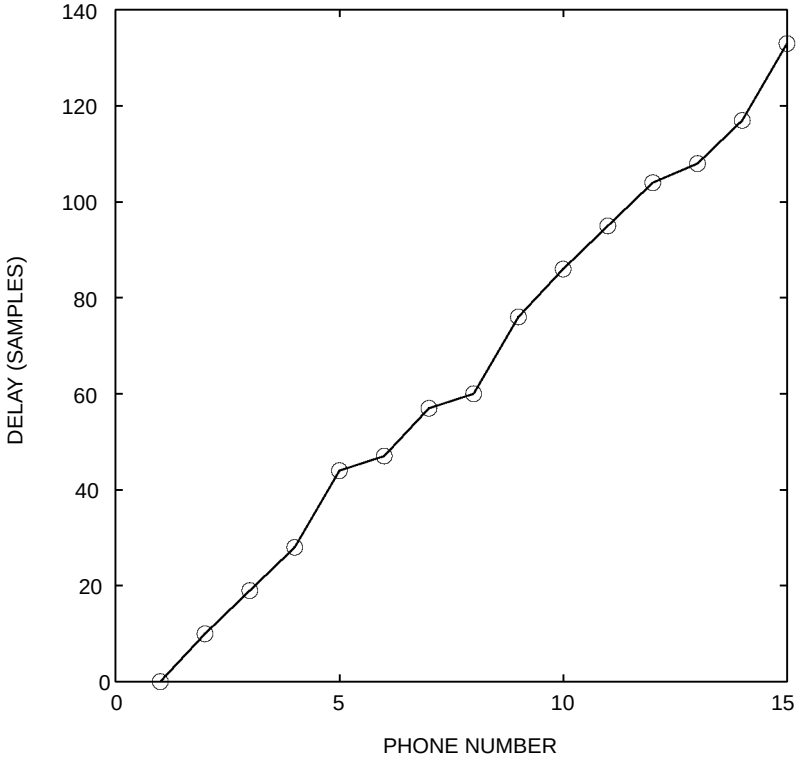

Figure 12. G201500, LF array.

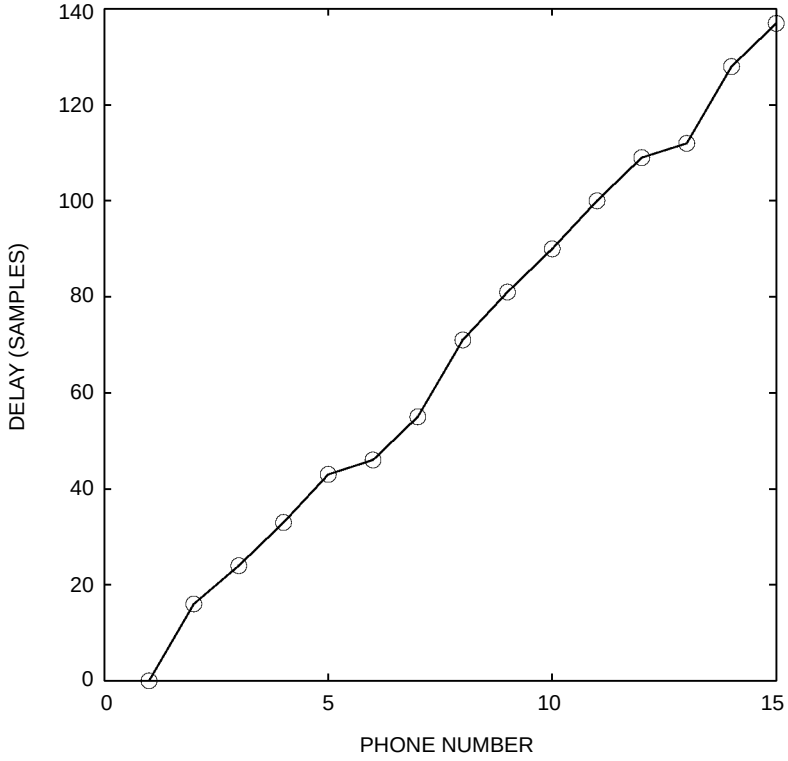

Figure 13. G201800, LF array.

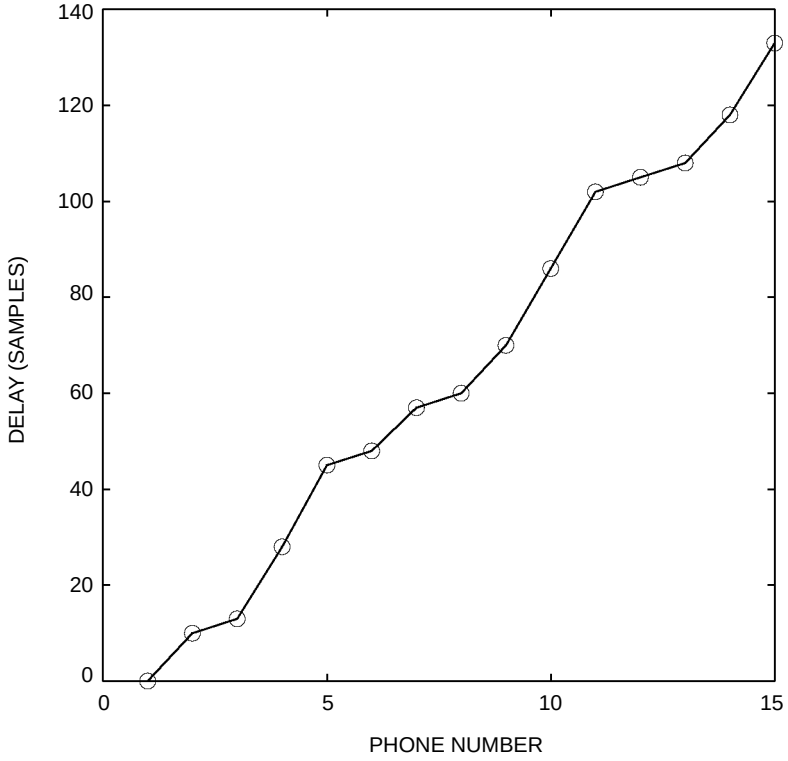

Figure 14. G201900, LF array.

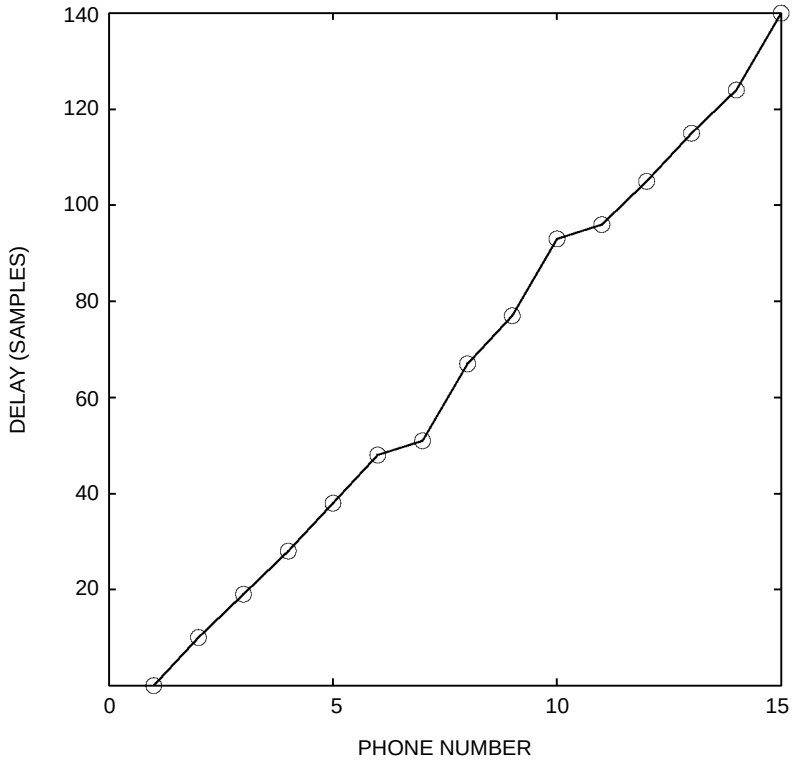

Figure 15. G202100, LF array.

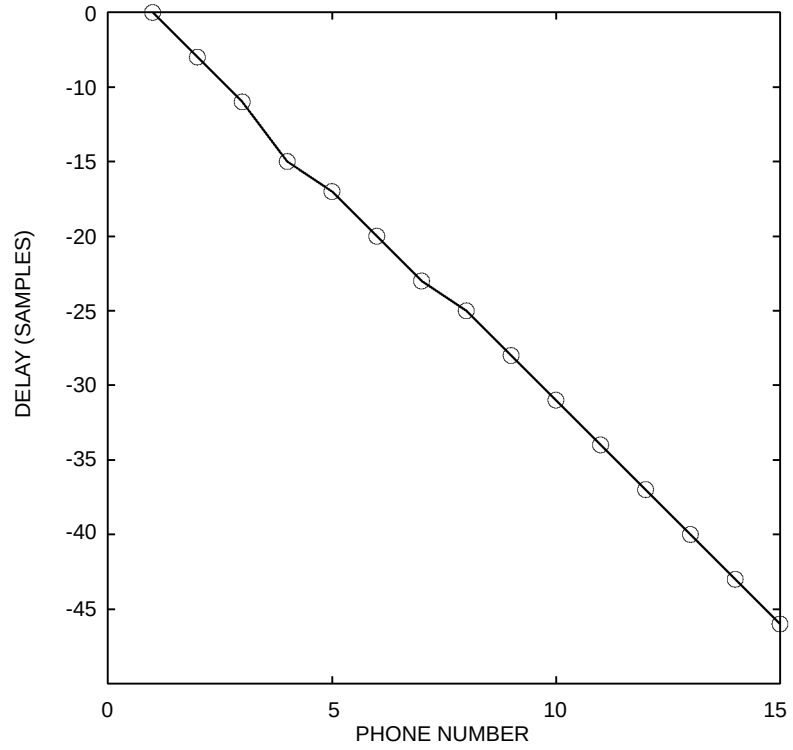

Figure 16. G204440, LF array.

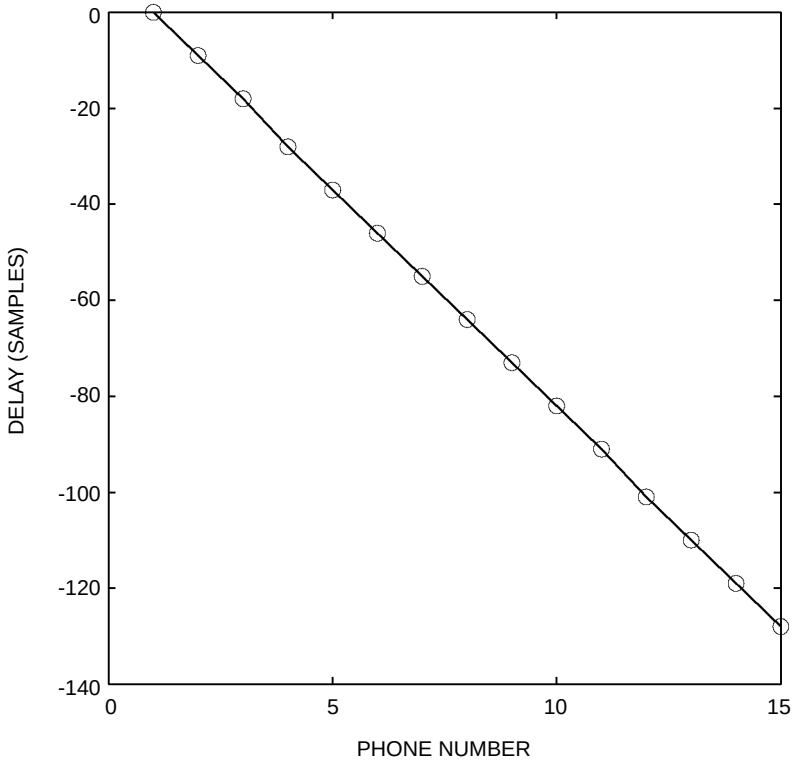

Figure 17. G220500, LF array.

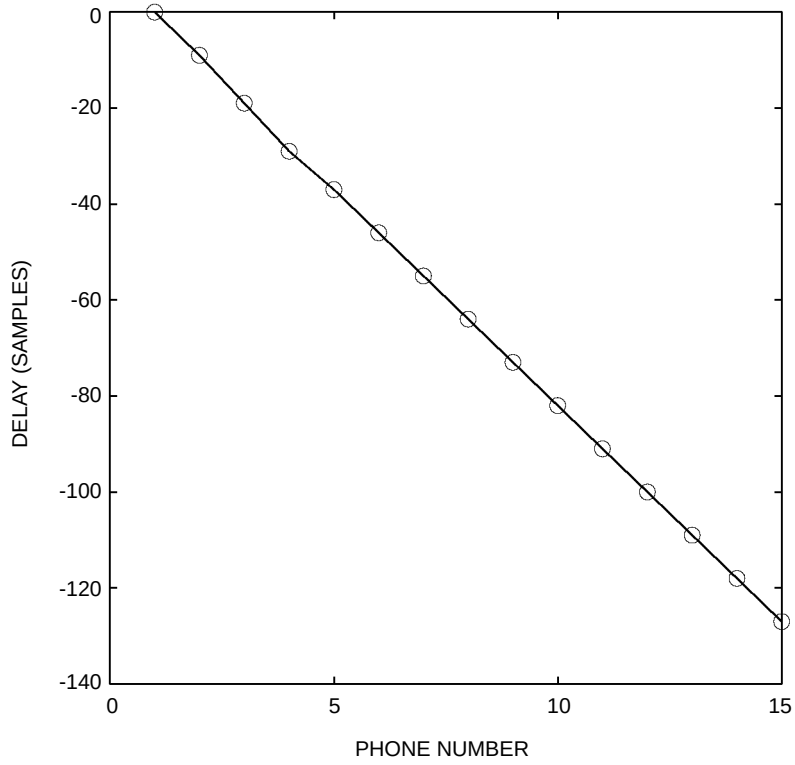

Figure 18. G220540, LF array.

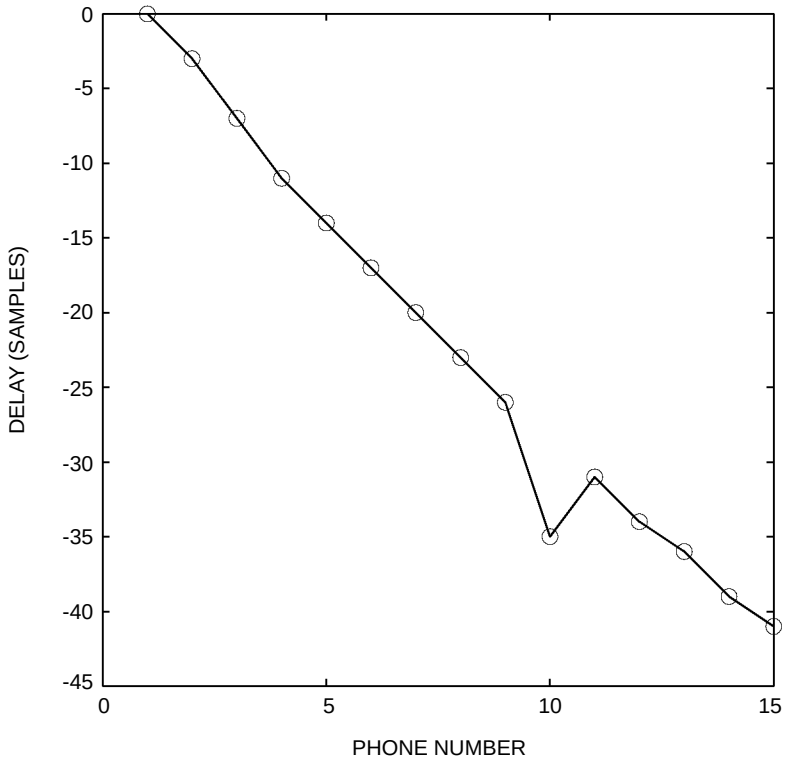

Figure 19. G22900, LF array.

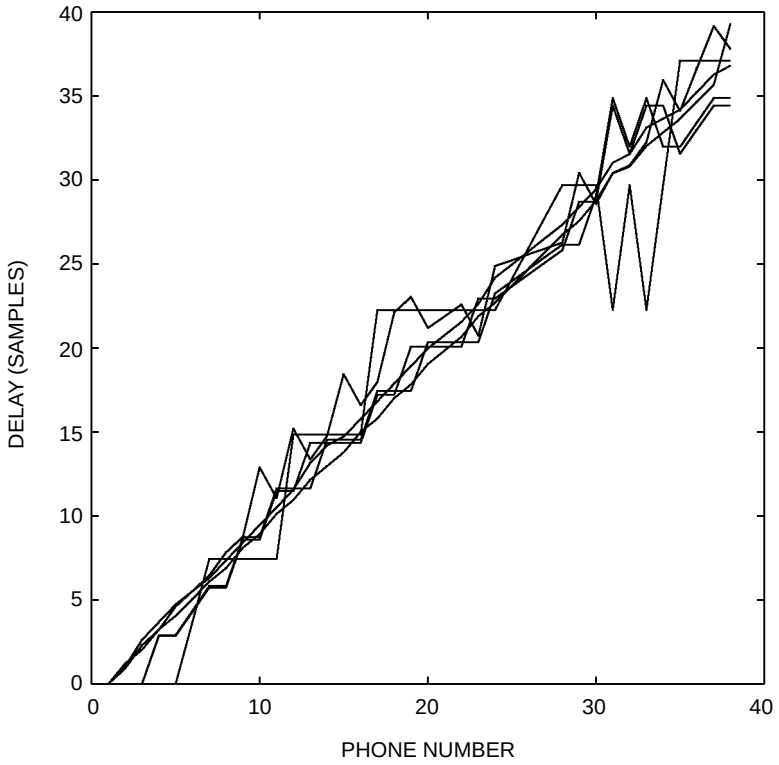

Figure 20. HF array, six trials.

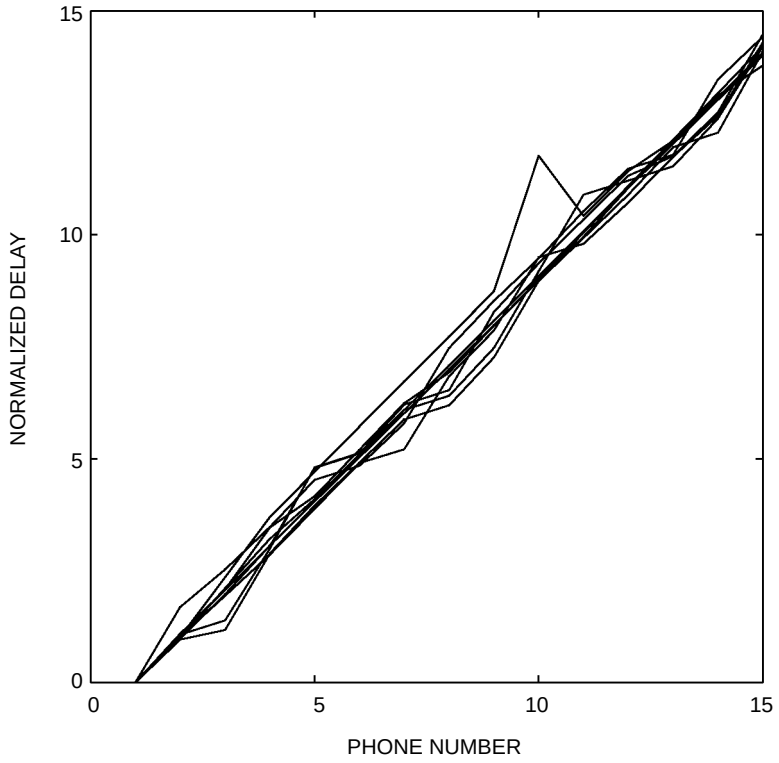

Figure 21. LF array, nine trials.

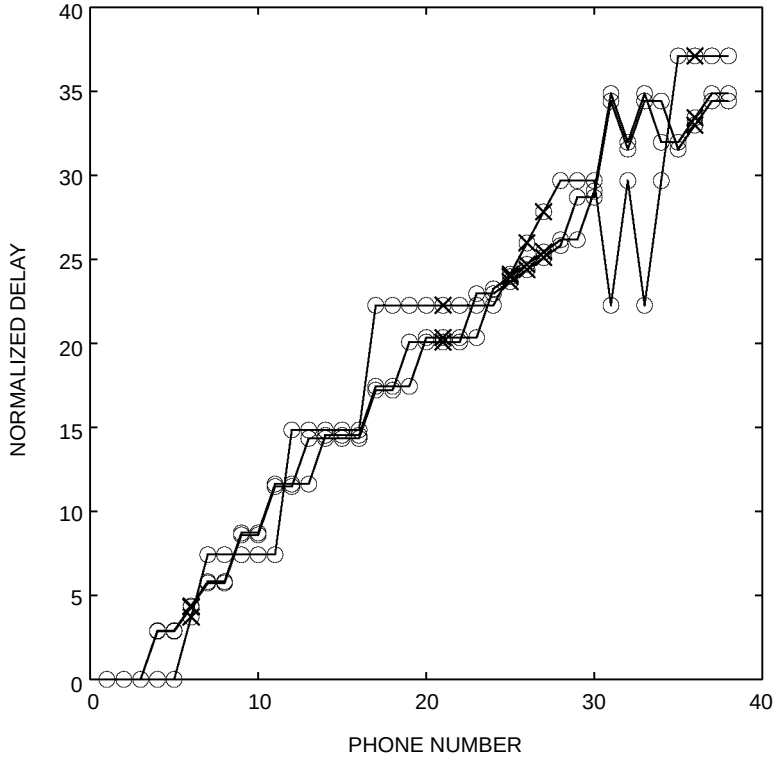

Figure 22. HF array, G201500 G201900 G204040.

Since the normalizing process amounts to rotating the best–fit line to a slope of 1, a comparison can be made regarding how close the data is to that line. Figure 23 shows the phone-by-phone difference between the slope-normalized data and a line of slope 1 for the high-frequency array. Figure 24 is a corresponding look at the low–frequency array.

Figure 25 is identical to figure 23 except the differences from trial G204040 are inverted to reflect the presumption that the arrival was from the other side. This shows considerable agreement with the remainder of the data trials on this array. This information is used to "correct" the normalized slope depiction of G204040 (flipping the deviations to the other side of the best-fit line), and is shown in figure 26.

ARRAY SPACING RELATIVE TO SAMPLE PERIOD

A comparison of the data on the two arrays, with spacing differing by two octaves, can be used to draw more general conclusions. The current sample rate, when used with the 160–Hz array, is roughly equivalent to using a sample rate 2 octaves higher with the 640–Hz array. Clearly the quantization of the arrival times is less of a problem when f_s/f_a is larger. Compare, for example, figures 7 and 17, which are recorded from similar angles.

More precisely, consider the consistency of the measurements for the two arrays. The mean of the slope–normalized data for array #1 (G204040 flipped) is shown in figure 27. The mean of the slope–normalized data for array #2 is shown in figure 28. As a measure of consistency, the deviations from the mean for the two arrays are plotted in figures 29 and 30. The standard deviation of the measurements on array #1 is 1.545. On array #2, the standard deviation is 0.372. Note that the ratio of these two values is practically identical to the ratio of the frequencies of the two arrays.

BANDWIDTH OF PULSE

The results from the high–bandwidth and low–bandwidth pulses were compared. Average variance was 0.71 for the high–bandwidth pulse and 2.36 for the low–bandwidth pulse. However, much of the difference is attributed to one extreme outlier (G204040) of the three trials using the low–bandwidth pulse. Since the effect of bearing relative to the source is already demonstrated, and the few samples available are not uniformly distributed across bearing, no conclusion should be drawn regarding bandwidth of the pulse.

EXTRANEOUS SOUNDS AS LOCALIZATION SOURCES

As was noted in the discussion above, trial G204040 exhibited a useful signal from a direction other than where the known sources were located. This was seen on a few additional trials as well.

Figure 31 shows the output of the replica correlation step of the procedure. This example is for G201400, and shows a good response for all phones on both arrays over a relatively short range of delays. (The absolute numbers associated with the delay are not meaningful; the time window is selected to present the relevant data at a reasonable level of detail.) This figure shows the nature of the response from the intended signal.

Contrast this figure with figure 32, which shows just the 15 phones of array #2 on trial G220500. Notice that two signals are arriving nearly simultaneously from different directions. If either one existed without the other, it would apparently be sufficient to perform element localization. This would seem to indicate that extraneous signals could be used for the purpose of element localization.

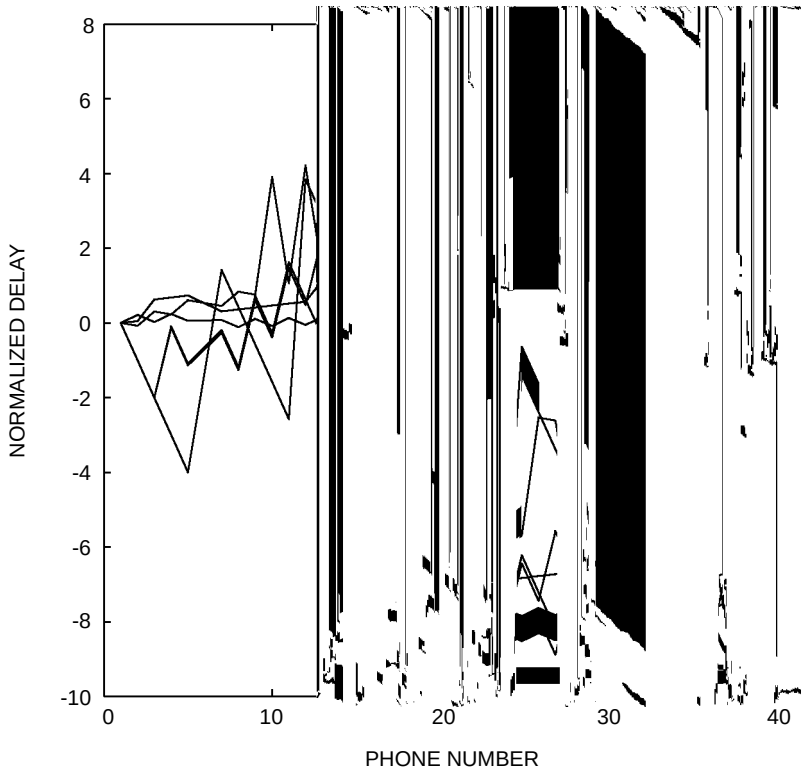

Figure 23. HF array, deviation from linear.

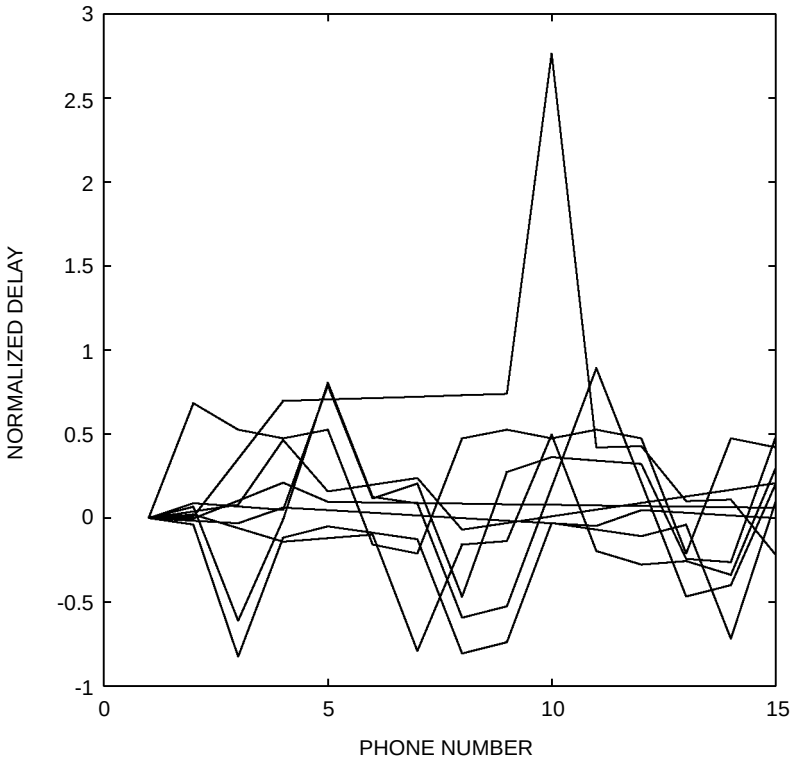

Figure 24. LF array, deviation from linear.

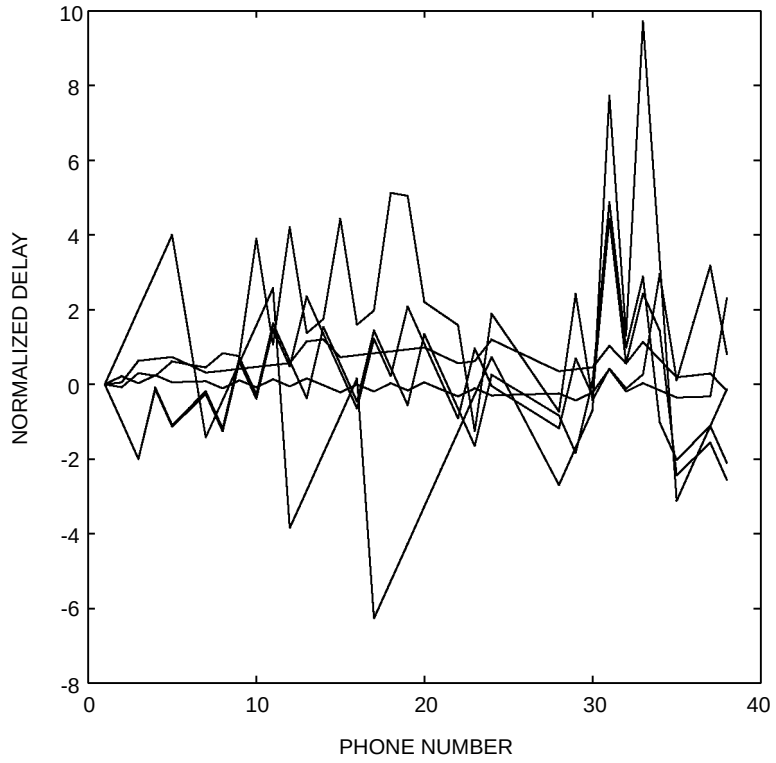

Figure 25. HF array, deviation from linear 2.

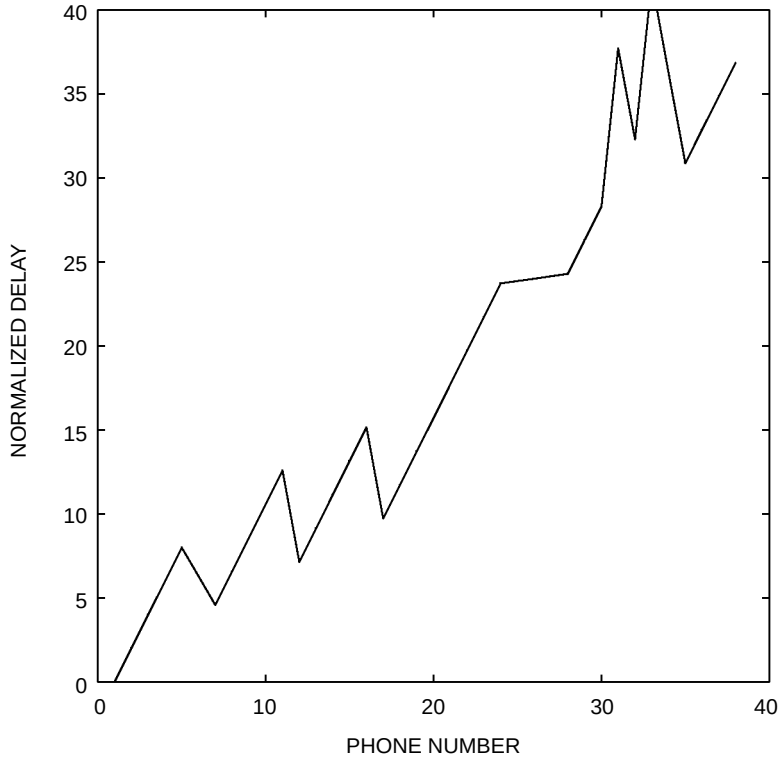

Figure 26. G204040, slopw normalized, flipped.

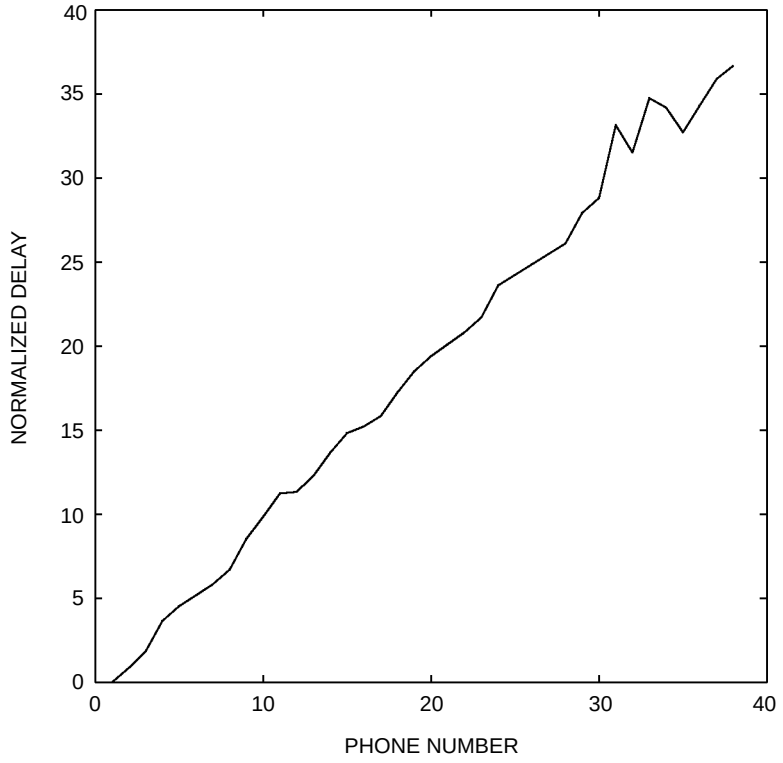

Figure 27. HF array, slopw normalized mean.

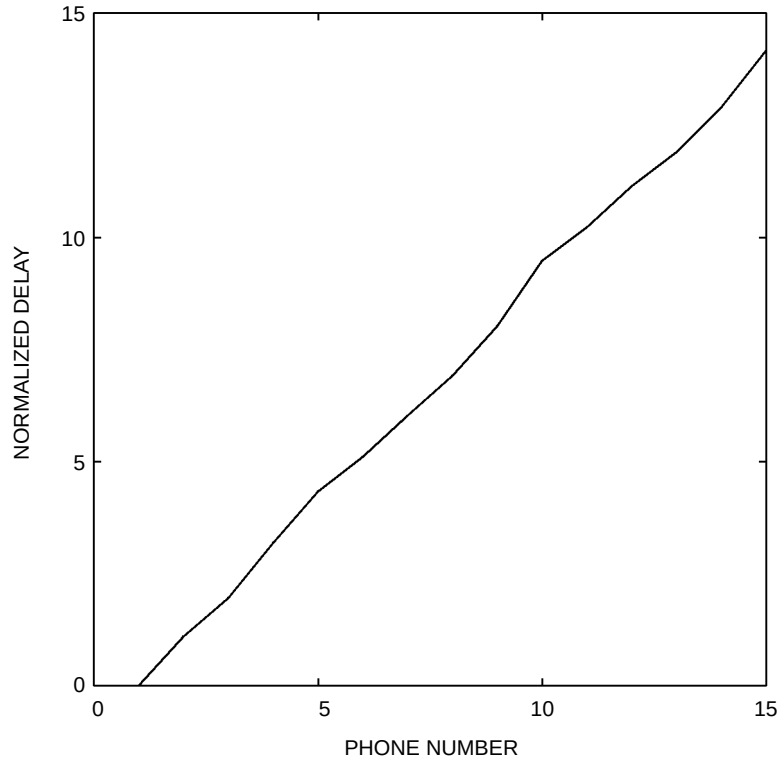

Figure 28. LF array, slope normalized mean.

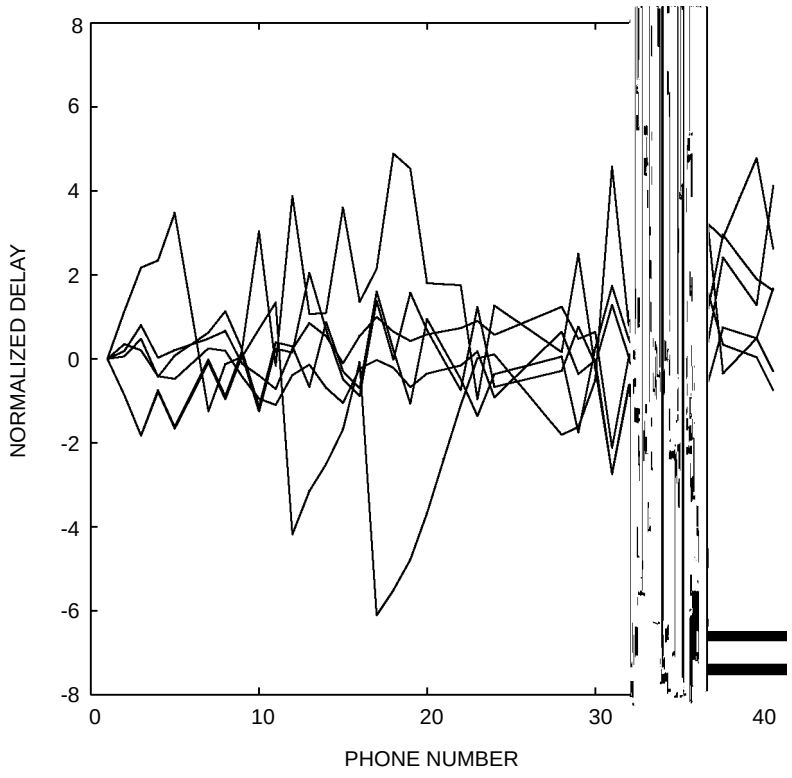

Figure 29. HF array, deviation from mean.

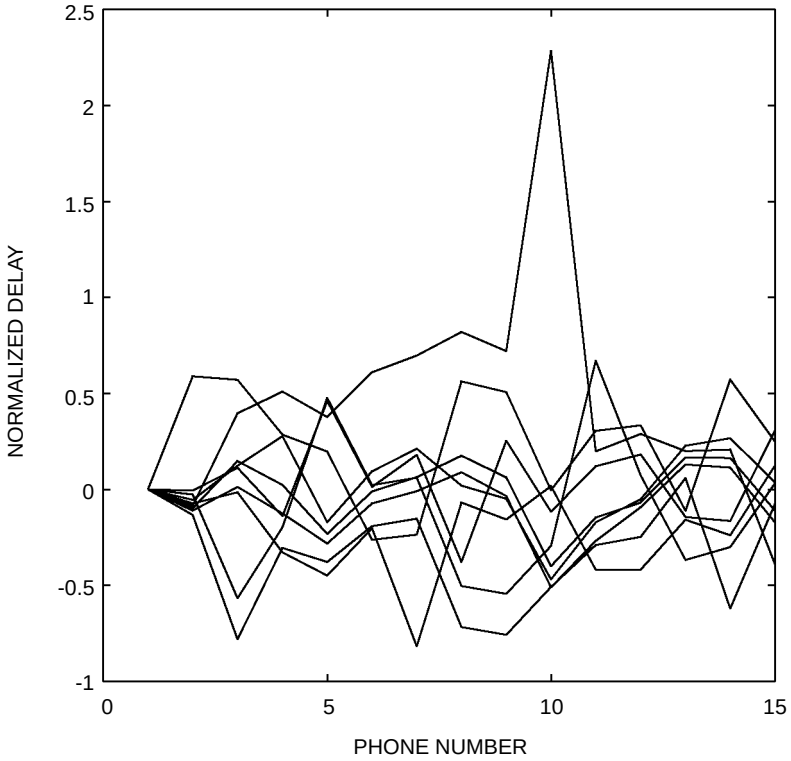

Figure 30. LF array, deviation from mean.

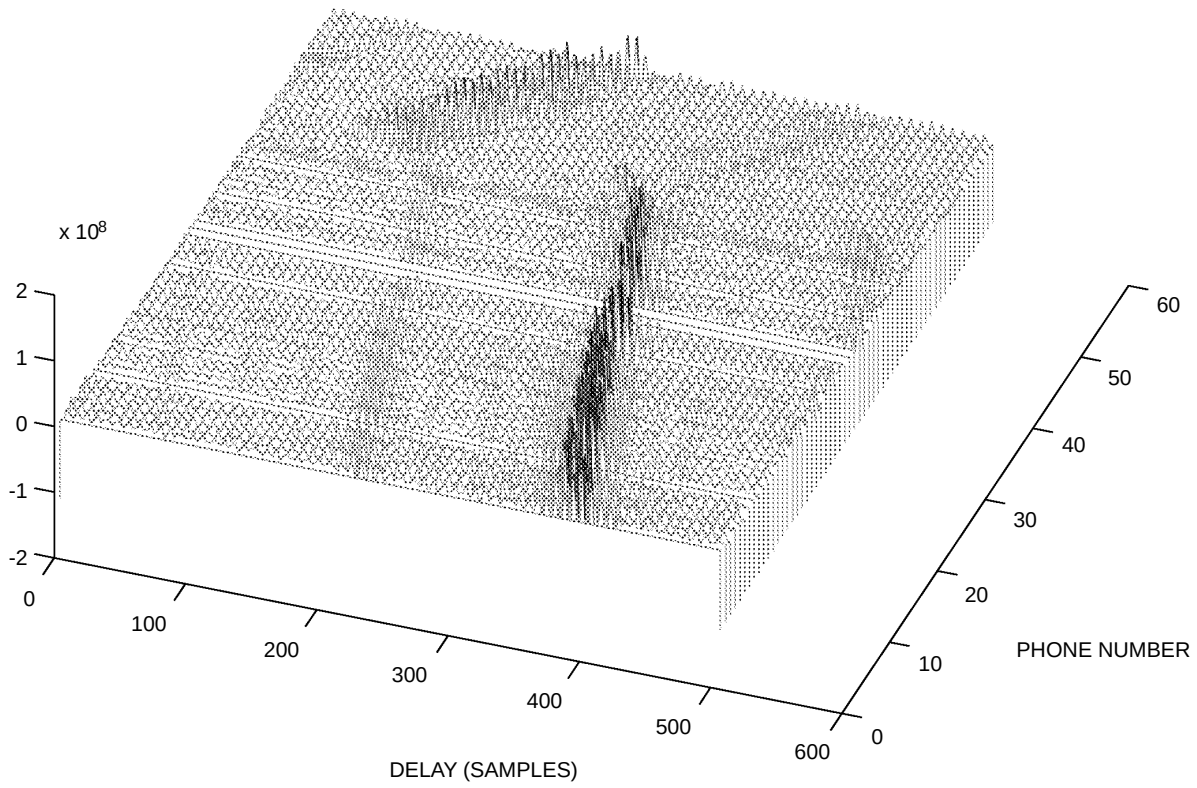

Figure 31. G201400, Correlation with signal from channel 6.

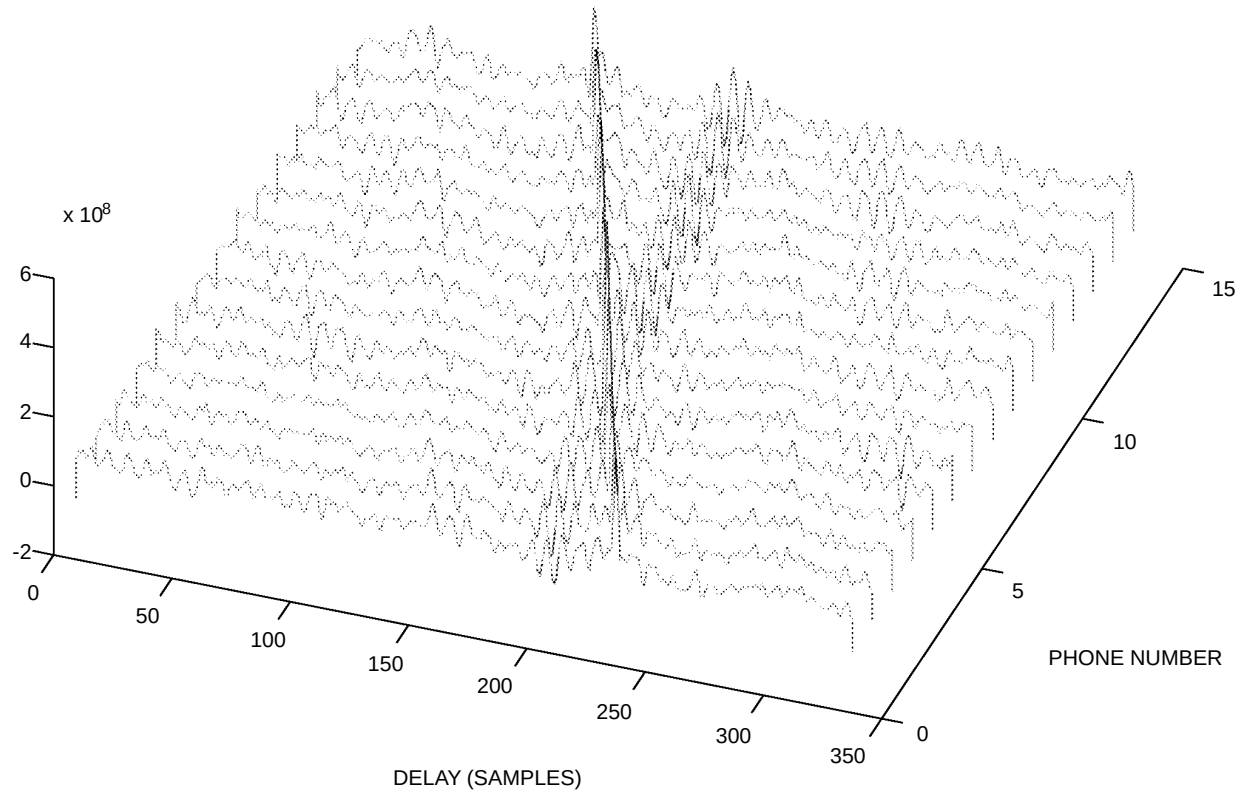

Figure 32. G220500, Correlation with signal from channel 48.

Figure 33 shows a longer time window of the same data trial as figure 32, as well as displaying all 58 channels. The high coherence between the arrays that was exhibited in figure 31 (and others within a few minutes of it) is no longer seen. It seems that the conditions deteriorated in the nearly 2 hours between these trials. Figure 34 shows the correlation with a time-window of channel 37 that most likely includes the signal. Thus, it is seen that the coherence within each array remains good, although the coherence between them is poor. Figure 35 looks very similar, but it uses a different and disjoint time-window from channel 2 as a replica; thus, it is believed to be a response due to an extraneous signal. This suggests that the signal and noise emanate from the same direction. One scenario consistent with this fact is the possibility that engine noise or cavitation from the boat, which was used to deploy the sources, is acting as the extraneous sound source.

Figure 36 presents a depiction of how good the noise coherence is across array #1. This is the same data as in figure 35, but the viewing angle has been altered to present a side view so the relative heights of the peaks can be seen.

Another example of two signals arriving from different angles at nearly the same time is seen in figure 37. The signal in this case is nearly broadside, while the extraneous response is close to end-fire. Using a later time–window of the same channel as a replica, the noise is still seen, but the signal no longer exists. See figure 38.

In the same pattern as figure 29, the deviation of the measurments from the unintended signals from previously calculated mean of the controlled signals is plotted in figure 39. The agreement with the other measurements is excellent These two trials exhibit a standard deviation of only 0.482. Thus, the signals we acquired by chance seem to work every bit as well as the signals we tried hard to create.

CONCLUSION

The concept of processing employed was consistent enough to warrant further interest. The method is not reliable enough that a single measurement provides sufficient confidence to be used as corrections to a beamformer. However, averages of about half a dozen measurements appear to have considerable consistency.

The deviations between measurements are attributed largely to quantization of the signal. Further analysis could validate the possibility of interpolating the existing data to a higher sample rate. Thus, the data may not need to be recorded at a higher sample rate, just interpolated prior to processing. The conclusion that was drawn about bearing from source to array (endfire is preferred to broadside) is also based on time quantization.

Extraneous sources of acoustic energy were shown to be of comparable utility in localization of the array elements. This also warrants further investigation when the array is redeployed. Controlled testing of broadband propulsion noise at various ranges and bearings from the array would provide data necessary to decide if such a crude sound source is acceptable.

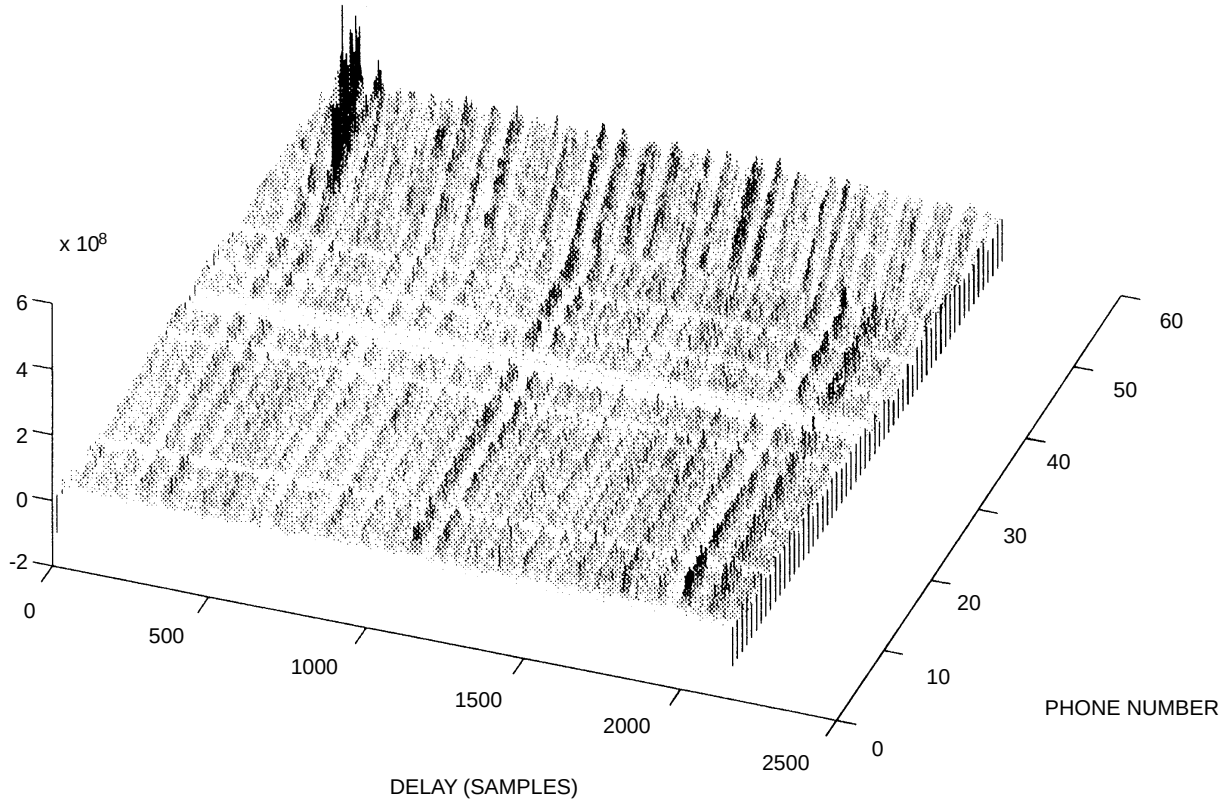

Figure 33. G220500, Correlation with signal from channel 48.

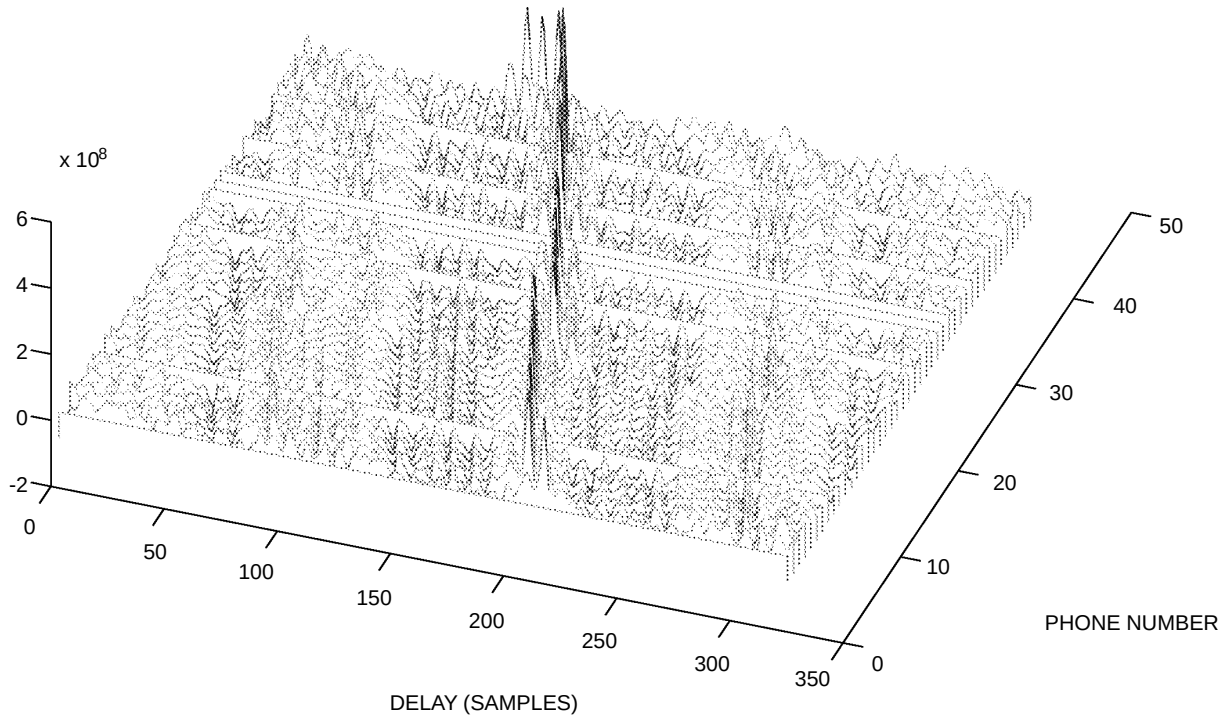

Figure 34. G220500, Correlation with signal from channel 37.

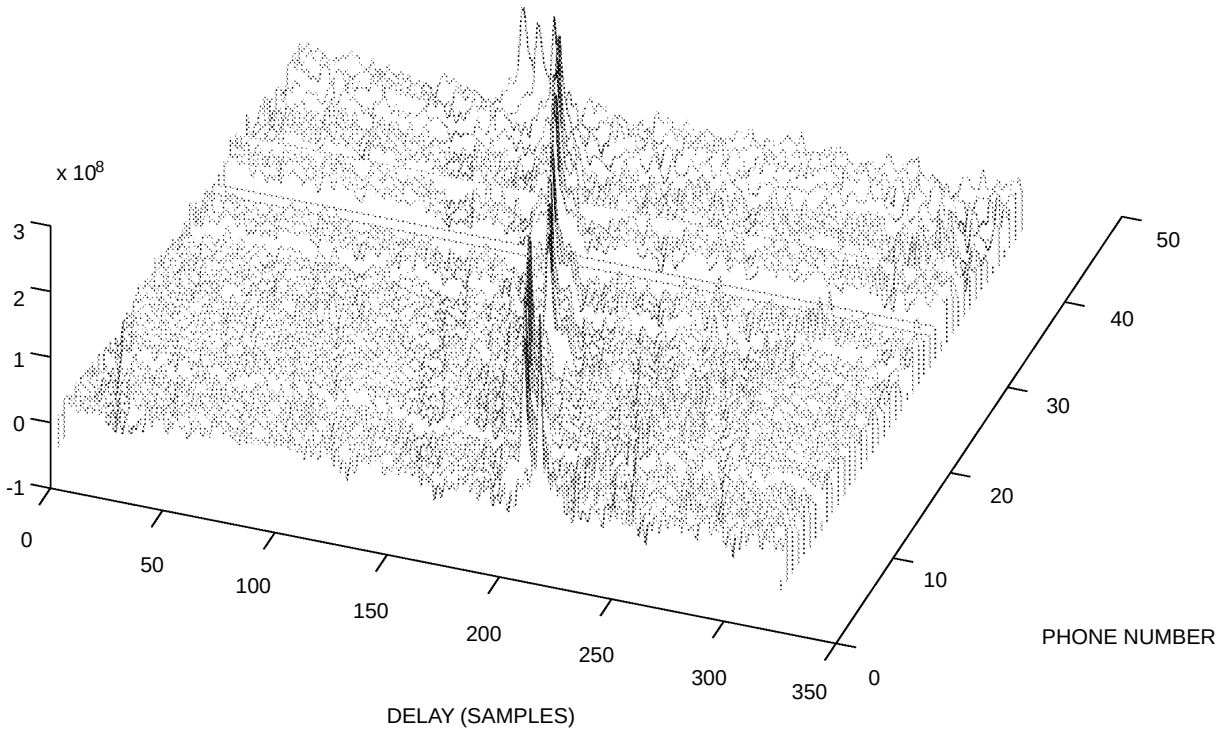

Figure 35. G220500, Correlation with noise from channel 2.

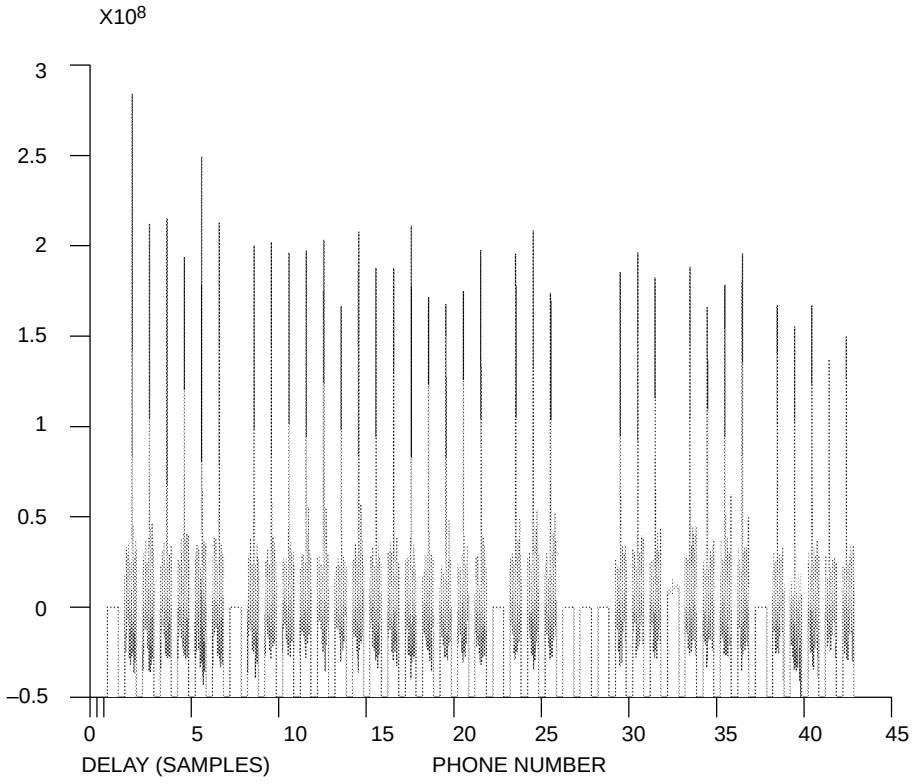

Figure 36. G220500, Correlation with noise from channel 2.

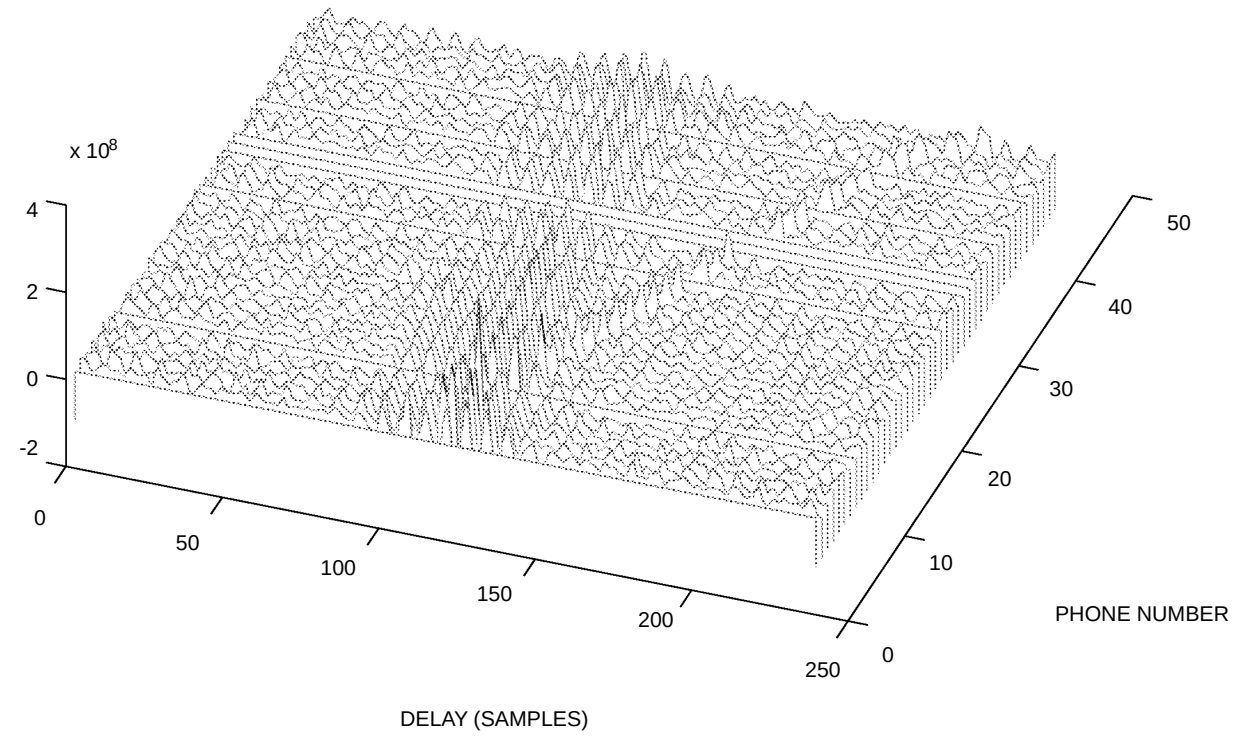

Figure 37. G203100, Correlation with signal from channel 6.

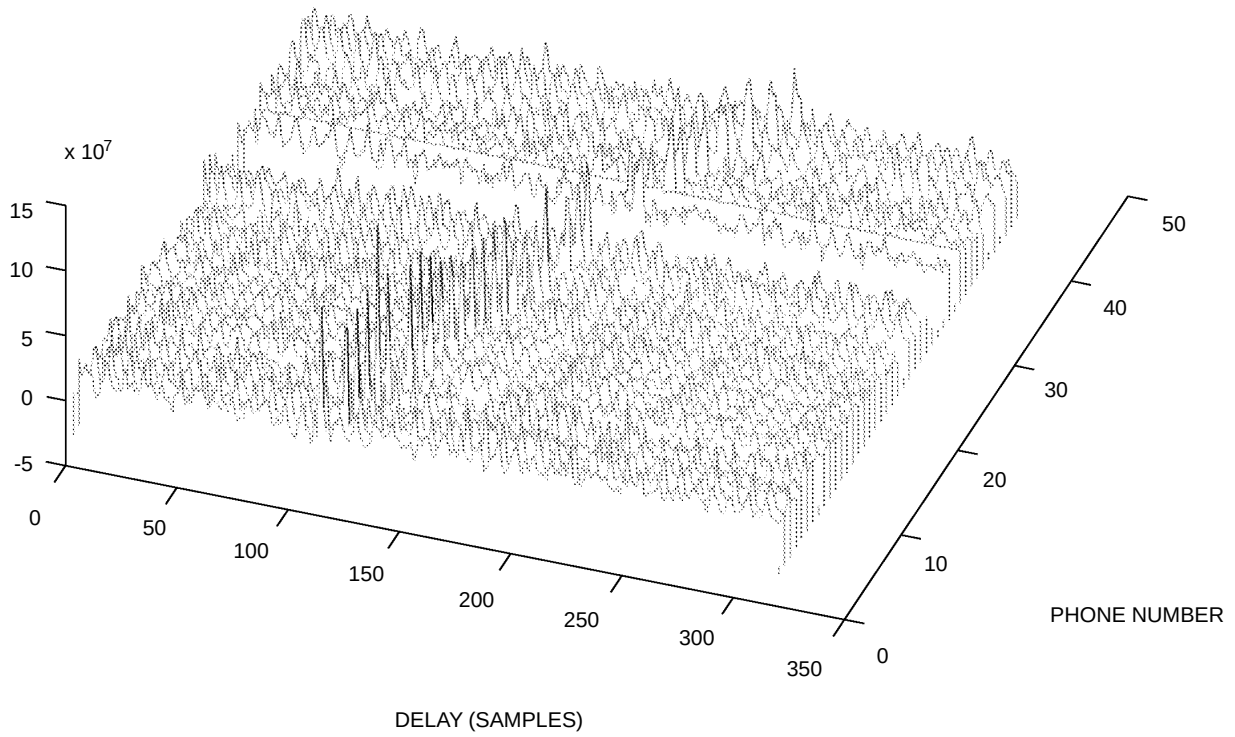

Figure 38. G203100, Correlation with noise from channel 6.

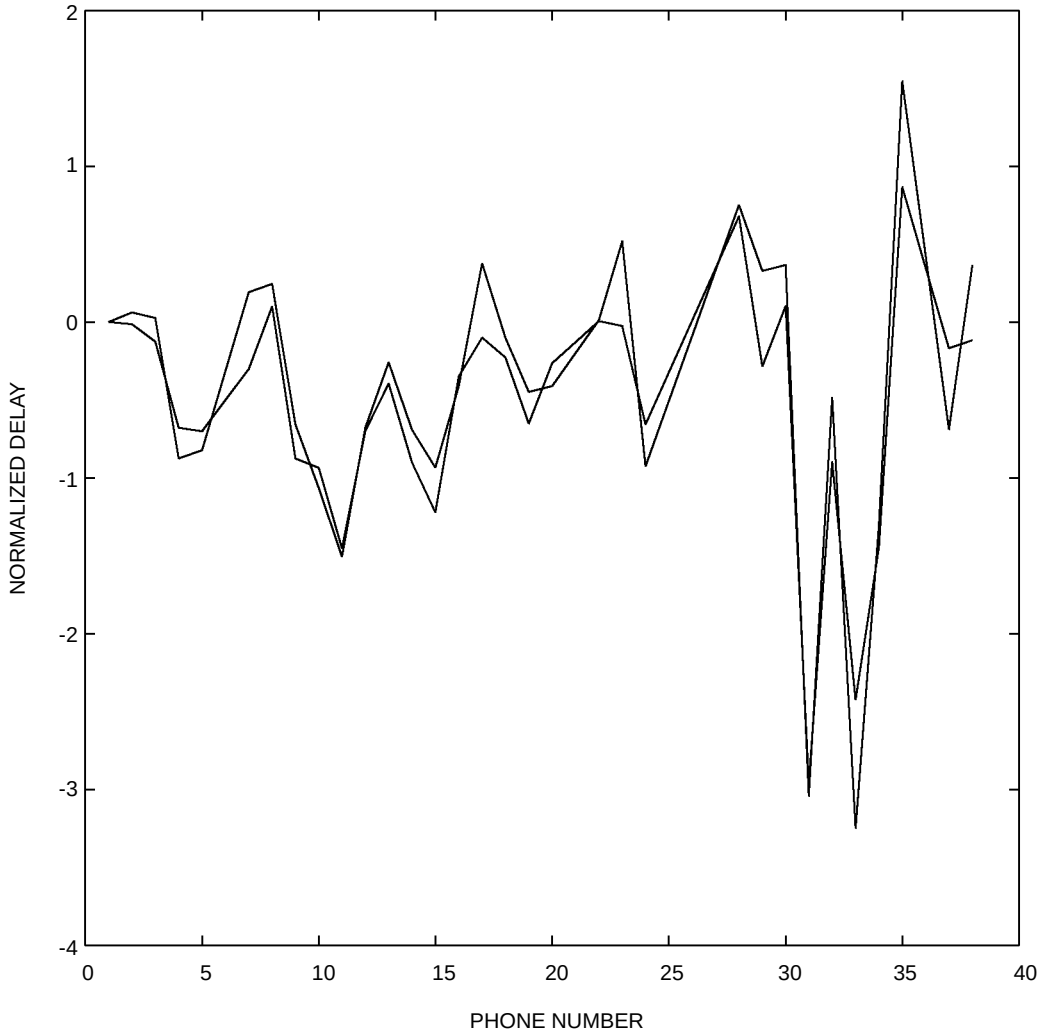

Figure 39. HF array, deviation from mean, noise measurements.

NOTATION

Matrices are denoted by bold–faced capital letters, e.g., $\mathbf{A}$. Indices to the rows and columns of a matrix are i and j respectively.

Vectors (either row or column vectors) are represented by bold–faced lower-case letters, e.g., $\mathbf{b}$. Consistent with the matrix notation, elements of a row vector are subscripted with j, and elements of a column vector are subscripted with i. If a vector is a subset of a matrix, the letter used will be the same, e.g., $\mathbf{c_i}$ is a row of $\mathbf{C}$.

Scalars are plain text, e.g., f or T. If a scalar is an element of a matrix, it will be upper-case with two subscripts (D_{ij}), and if it is an element of a vector it will be lower–case and have a single subscript (f_i).

REFERENCE

1. Williams, J.R., *Phone Location System (PLS) San Diego Sea Tests 14–16 September 1994 with EDM–1E String Sensors*, 10 Oct 1994, DRS Doc # 385.

REPORT DOCUMENTATION PAGE

Form Approved
OMB No. 0704-0188

1. AGENCY USE ONLY *(Leave blank)*	2. REPORT DATE	3. REPORT TYPE AND DATES COVERED

4. TITLE AND SUBTITLE	5. FUNDING NUMBERS

6. AUTHOR(S)	
T. J. Pastore	

7. PERFORMING ORGANIZATION NAME(S) AND ADDRESS(ES)	8. PERFORMING ORGANIZATION REPORT NUMBER
Naval Command, Control and Ocean Surveillance Center (NCCOSC) RDT&E Division San Diego, California 92152–5001	

9. SPONSORING/MONITORING AGENCY NAME(S) AND ADDRESS(ES)	10. SPONSORING/MONITORING AGENCY REPORT NUMBER

11. SUPPLEMENTARY NOTES

12a. DISTRIBUTION/AVAILABILITY STATEMENT	12b. DISTRIBUTION CODE

13. ABSTRACT *(Maximum 200 words)*

This report describes our procedure and initial study of the feasibility and practicality of using a frequency modulated (FM) chirp to

14. SUBJECT TERMS	15. NUMBER OF PAGES
	16. PRICE CODE

17. SECURITY CLASSIFICATION OF REPORT	18. SECURITY CLASSIFICATION OF THIS PAGE	19. SECURITY CLASSIFICATION OF ABSTRACT	20. LIMITATION OF ABSTRACT
UNCLASSIFIED	UNCLASSIFIED	UNCLASSIFIED	SAME AS REPORT

21a. NAME OF RESPONSIBLE INDIVIDUAL	21b. TELEPHONE *(include Area Code)*	21c. OFFICE SYMBOL
T.J. Pastore	(619) 553–6262	Code 532

INITIAL DISTRIBUTION

Code 0012	Patent Counsel	(1)
Code 0271	Archive/Stock	(6)
Code 0274	Library	(2)
Code 50	H. O. Porter	(1)
Code 53	D. W. Murphy	(1)
Code 531	B. Marsh	(1)
Code 532	C. D. Metz	(1)
Code 532	R. W. Floyd	(1)
Code 532	T. J. Pastore	(5)
Code 714	G. Davis	(1)

Defense Technical Information Center
Alexandria, VA 22304–6145 (4)

NCCOSC Washington Liaison Office
Washington, DC 20363–5100

Center for Naval Analyses
Alexandria, VA 22302–0268

Navy Acquisition, Research and Development
Information Center (NARDIC)
Arlington, VA 22244–5114

GIDEP Operations Center
Corona, CA 91718–8000

OST
Fort Washington, MD 20744

DRS Military Systems
Oakland, NJ 07436 (2)

SAIC
San Diego, CA 92121

SAIC
McLean, VA 22102